

The prebiotic molecular inventory of Serpens SMM1:

II. The building blocks of peptide chains

Niels F.W. Ligterink,^{*,†} Aida Ahmadi,[‡] Bijaya. Luitel,[¶] Audrey Coutens,[§] Hannah Calcutt,^{||} Łukasz Tychoniec,[⊥] Harold Linnartz,[#] Jes K. Jørgensen,[@] Robin T. Garrod,[△] and Jordy Bouwman^{‡,▽}

[†]*Physics Institute, University of Bern, Sidlerstrasse 5, 3012 Bern, Switzerland*

[‡]*Leiden Observatory, Leiden University, PO Box 9513, 2300 RA Leiden, The Netherlands*

[¶]*Yale-NUS College, #01-220, 16 College Avenue West, 138527, Singapore*

[§]*Institut de Recherche en Astrophysique et Planétologie, Université de Toulouse, UPS-OMP, CNRS, CNES, 9 av. du Colonel Roche, 31028 Toulouse Cedex 4, France*

^{||}*Institute of Astronomy, Faculty of Physics, Astronomy and Informatics, Nicolaus Copernicus University, Grudziadzka 5, 87-100 Torun, Poland*

[⊥]*ESO, Karl-Schwarzschild-Strasse 2, 85748 Garching bei München, Germany*

[#]*Laboratory for Astrophysics, Leiden Observatory, Leiden University, PO Box 9513, 2300 RA Leiden, The Netherlands*

[@]*Centre for Star and Planet Formation, Niels Bohr Institute & Natural History Museum of Denmark, University of Copenhagen, Øster Voldgade 5–7, 1350 Copenhagen K., Denmark*

[△]*Departments of Chemistry and Astronomy, University of Virginia, Charlottesville, VA 22904, USA*

[▽]*Laboratory for Atmospheric and Space Physics, Department of Chemistry, Institute for Modeling Plasma, Atmospheres, and Cosmic Dust (IMPACT), University of Colorado, Boulder, CO 80303, USA*

E-mail: niels.ligterink@unibe.ch

Abstract

This work aims to constrain the abundances of interstellar amides, by searching for this group of prebiotic molecules in the intermediate-mass protostar Serpens SMM1-a. ALMA observations are conducted toward Serpens SMM1. A spectrum is extracted toward the SMM1-a position and analyzed with the CASSIS line analysis software for the presence of characteristic rotational lines of a number of amides and other molecules. NH_2CHO , $\text{NH}_2\text{CHO } \nu_{12}=1$, $\text{NH}_2^{13}\text{CHO}$, $\text{CH}_3\text{C(O)NH}_2 \nu=0,1$, CH_2DOH , CH_3CHO , and $\text{CH}_3\text{C(O)CH}_3$ are securely detected, while *trans*- NHDCHO , NH_2CDO , $\text{CH}_3\text{NHCHO } \nu=0,1$, CH_3COOH , and HOCH_2CHO are tentatively identified. The results of this work are compared with detections presented in the literature. A uniform $\text{CH}_3\text{C(O)NH}_2/\text{NH}_2\text{CHO}$ ratio is found for a group of interstellar sources with vast physical differences. A similar ratio is seen for CH_3NHCHO , based on a smaller data sample. The D/H ratio of NH_2CHO is about 1–3% and is close to values found in the low-mass source IRAS 16293–2422B. The formation of $\text{CH}_3\text{C(O)NH}_2$ and NH_2CHO is likely linked. Formation of these molecules on grain surfaces during the dark cloud stage is a likely scenario. The high D/H ratio of NH_2CHO is also seen as an indication that these molecules are formed on icy dust grains. As a direct consequence, amides are expected to be present in the most pristine material from which planetary systems form, thus providing a reservoir of prebiotic material.

Introduction

Peptide chains, amino acids connected by a $\text{R}_1\text{-C(=O)N-R}_2\text{R}_3$ group, are an essential component of life as we know it, since these molecules can fold into proteins, which, in turn, are the engines that life runs on. During protein biosynthesis, ribosomes catalyze condensation reactions between amino acids, resulting in the formation of a peptide bond, also called an amide, and a water molecule¹. However, to understand how the peptide chains formed before life was present, abiotic processes need to be studied.

Several mechanisms have been proposed for abiotic peptide synthesis, involving catalysis by minerals², in hydrothermal vents^{3,4}, with UV light⁵, or by impact shocks⁶. The last mechanism is particularly interesting, because it hints at an extraterrestrial origin of peptide chains. In fact, in the laboratory it has been demonstrated that dipeptides such as glycine-glycine and alanine-leucine can form in interstellar ice analogues⁷. Incorporation of these interstellar peptides into planetary building material and subsequent delivery by impactors like comets, could have helped start life on the Early Earth.

To understand interstellar peptide chemistry, observations of star-forming regions can help elucidate how these molecules form. While observations of dipeptides and larger molecules are beyond current capabilities, several peptide-like molecules have been detected with radio and mm-wave observations. Formamide (NH_2CHO) has the same chemical structure as a peptide bond and is the simplest peptide-like molecule. It is the first peptide-like molecule to be detected in the interstellar medium (ISM) and is routinely found in extraterrestrial environments, ranging from star-forming regions to comets⁸⁻¹⁰. Since the detection of formamide, several other peptide-like molecules have been detected, such as acetamide ($\text{CH}_3\text{C}(\text{O})\text{NH}_2$)¹¹, N-methylformamide (CH_3NHCHO)¹²⁻¹⁵, and urea (also known as carbamide, $\text{NH}_2\text{C}(\text{O})\text{NH}_2$)^{13,16}. Searches for and tentative detections of several other peptide-like molecules have been reported, such as glycolamide ($\text{HOCH}_2\text{C}(\text{O})\text{NH}_2$)^{15,17}, cyanofornamide ($\text{N}_2\text{C}(\text{O})\text{CN}$)¹⁵, and propionamide ($\text{CH}_3\text{CH}_2\text{C}(\text{O})\text{NH}_2$)¹⁸.

Observations of these molecules provide insight into the chemical processes that result in their formation, which, in turn, indicate whether larger amides or even peptides are expected to form in the ISM. For example, correlations found between interstellar abundances of NH_2CHO and $\text{CH}_3\text{C}(\text{O})\text{NH}_2$ hint that there is a physico-chemical link between these two molecules^{15,19}. The similarity in the ratios of these molecules in a sample of sources with very different physical characteristics, is explained by an early formation during the star formation cycle, presumably on ice-coated interstellar dust grains. Furthermore, this observation hints that these molecules form in related chemical reactions or even directly act as a precursor.

While observations of peptide-like molecules are valuable, detections of these molecules are still relatively sparse. Furthermore, detections are biased toward luminous high-mass protostars and star-forming regions. Peptide-like molecules detected toward low-mass protostars almost exclusively consists of NH_2CHO , with as only exception a tentative detection of $\text{CH}_3\text{C}(\text{O})\text{NH}_2$ toward the low-mass protostar IRAS 16293–2422B²⁰. Identifications toward low-mass and Sun-like protostars will extend our knowledge of interstellar amide formation.

In this publication, observations of Serpens SMM1-a (hereafter SMM1-a), an intermediate-mass Class 0 protostar in the Serpens cloud ($D \approx 436.0 \pm 10 \text{ pc}^{21}$), are used. In particular, the outflows of the SMM1 region are well studied^{22,23}, but also its molecular inventory^{24–27}. The comparatively high luminosity of $\sim 100 L_\odot$ makes this an interesting source in the low-end protostellar mass range to search for weak spectral lines of prebiotic and peptide-like molecules.

This work presents the first detection of NH_2CHO , $\text{CH}_3\text{C}(\text{O})\text{NH}_2$, and various isotopologues toward SMM1-a, combined with a tentative detection of CH_3NHCHO and upper limits of various other peptide-like molecules. The observations and analysis are presented in Sect. Observations & Analysis, followed by the results in Sect. Results. These results are discussed in Sect. Discussion and conclusions are given in Sect. Conclusions.

Observations & Analysis

The observations of Serpens SMM1 and the analysis methods are introduced in Ligterink et al.²⁶ and only a brief overview will be given here.

Observations of SMM1 were conducted on 27-03-2019 in ALMA cycle 6 for project #2018.1.00836.S (PI: N.F.W. Ligterink). The source was observed toward the phase centre $\alpha_{\text{J2000}} = 18:29:49.80$ $\delta_{\text{J2000}} = +01:15:20.6$ in select frequency windows between 217.59 and 235.93 GHz. The spectral resolution was 488.21 kHz ($\sim 0.33 \text{ km s}^{-1}$, several bands between 217.59 and 233.65 GHz) and 1952.84 kHz ($\sim 1.25 \text{ km s}^{-1}$, between 234.06 and 235.93 GHz)

for the continuum band, while the spatial resolution was $1.32'' \times 1.04''$. The spectrum of the SMM1-a hot core was extracted toward position $\alpha_{\text{J2000}} = 18:29:49.793$, $\delta_{\text{J2000}} = +1.15.20.200$ in a beam of $1.32'' \times 1.04''$. The background temperature was determined to be ~ 5 K.

The CASSIS¹ line analysis software was used to analyze the spectra. Line lists taken from the Cologne Database for Molecular Spectroscopy (CDMS)^{29–31}, the JPL database for molecular spectroscopy³², and from the literature were used to identify and fit spectral lines. These databases are also used to identify the lines that are largely free of blending transitions originating from other molecules. Largely clean lines are defined as transitions that have an almost negligible contribution of a blending transition (approximately 10% of the observed line intensity) or only blend with another species in the wing of the transition. Only largely clean lines were used for subsequent line fitting. A synthetic spectrum consisting of the emission of all 26 securely and tentatively detected species detected toward SMM1-a in this work and in Ligterink et al.²⁶ was generated to check against and verify that detected lines were unblended. An overview of the spectroscopic data of the species discussed in this paper are given in the spectroscopy supporting information section, Table 3.

For a given column density (N_{T}), excitation temperature (T_{ex}), source velocity (V_{LSR}), line width (ΔV), background temperature ($T_{\text{BG}} = 5.2$ K, derived from the average continuum flux density of $0.41 \text{ Jy beam}^{-1,26}$), and source size, which is assumed to be equal to the beam size ($\theta_{\text{source}} = 1.2''$), a synthetic spectrum was generated, assuming Local Thermodynamic Equilibrium (LTE) conditions. This synthetic spectrum was initially fit by-eye to the rotational lines identified in the observed spectrum. Next, a χ^2 minimization routine in combination with the Monte-Carlo Markov Chain (MCMC) algorithm was applied to find the best fit to the observed spectrum. The column density was given as a free parameter over two orders of magnitude around the by-eye fit column density, while $T_{\text{ex}} = 50 - 350$ K, $\Delta V = 1.0 - 4.0 \text{ km s}^{-1}$, and $V_{\text{LSR}} = 6.0 - 9.0 \text{ km s}^{-1}$. In certain cases, T_{ex} , ΔV , or V_{LSR} could not properly be fit and instead estimated values were given. In most cases, these estimates

¹Based on analysis carried out with the CASSIS software (<http://cassis.irap.omp.eu>; Vastel et al.²⁸). CASSIS has been developed by IRAP-UPS/CNRS.

were based on an average of values found for other molecules where a proper fit was possible or based on related species, for example isotopologues.

A secure identification is based on the detection of at least 3 largely unblended lines for species that have prominent spectral lines and are routinely observed in interstellar observations (e.g., NH_2CHO , CH_3OH), while 5 or more lines are required to claim a detection of species that are less routinely observed or have comparatively weak spectral lines (e.g., $\text{CH}_3\text{C}(\text{O})\text{NH}_2$ or glycolaldehyde, HOCH_2CHO). If no lines are identified of a species, an upper limit is determined that is based on the 3σ noise level of a line of the species that is found in a line-free segment of the spectrum.

From the average continuum flux density ($0.41 \text{ Jy beam}^{-1,26}$), the H_2 column density can be estimated following equation^{33,34}:

$$N(\text{H}_2) = \frac{F_\nu R}{B_\nu(T_D)\Omega\kappa_\nu\mu m_H}, \quad (1)$$

where F_ν is the flux density, R the gas-to-dust mass ratio, $B_\nu(T_D)$ the planck function for dust temperature T_D , Ω the beam solid angle, κ_ν the dust absorption coefficient, μ the mean molecular weight, and m_H the atomic hydrogen mass. R is assumed to be 100, $\kappa_{220\text{GHz}} = 0.9 \text{ cm}^2 \text{ g}^{-1,35}$, and $\mu = 2.8$. The dust temperature is assumed to be coupled to the gas temperature. The excitation temperature of the dense gas tracer $\text{CH}_3\text{CN}^{26}$ is adopted, resulting in $T_D = 190 \text{ K}$. From this, a hydrogen column density of $N(\text{H}_2) = (1\pm 0.2)\times 10^{24} \text{ cm}^{-2}$ is estimated.

Results

In the SMM1-a spectrum several lines originating from amides are identified, leading to the secure detection of $\text{NH}_2\text{CHO } \nu_{12}=1$, $\text{CH}_3\text{C}(\text{O})\text{NH}_2 \nu=0,1$, $\text{NH}_2\text{CHO } \nu=0$, and $\text{NH}_2^{13}\text{CHO}$ (see Figs. 1 and 2 and supplementary information Figs. 7, 8, and 9, while $\text{CH}_3\text{NHCHO } \nu=0,1$, NH_2CDO , and *trans*- NHDCHO are tentatively identified (see Fig. 3 and supplementary

information Figs. 10 and 11). Moment 0 maps of the emission of selected NH_2CHO $\nu_{12}=1$, NH_2CDO , $\text{CH}_3\text{C}(\text{O})\text{NH}_2$ $\nu=0$, and CH_3NHCHO $\nu=0$ lines are shown in Fig. 4. These maps show compact emission of these amides toward the peak continuum of SMM1-a. The difference in the extent of the emission between the NH_2CHO isotopologues and the larger $\text{CH}_3\text{C}(\text{O})\text{NH}_2$ and CH_3NHCHO molecules, probably results from the lower line brightness of the latter two species, but may also be due to different chemical responses to the environment, for example the gas density³⁶. The spatial resolution of these observations is insufficient to resolve finer features in the distribution of these molecules throughout the source and to give a definitive answer to this question.

The excitation temperature could only be determined for $\text{CH}_3\text{C}(\text{O})\text{NH}_2$, $\nu=0$, albeit with a large error bar, at $T_{\text{ex}} = 235 \pm 80$ K. For the $\text{CH}_3\text{C}(\text{O})\text{NH}_2$, $\nu=1$ fit the excitation temperature of its ground vibrational state is adopted. The remaining species were fit with $T_{\text{ex}} = 200$ K, the average temperature that could be securely determined from the detected molecular species toward SMM1-a²⁶. Other excitation temperatures are possible, which can affect the derived column density. For T_{ex} of 100 to 300 K, temperatures that are generally realistic for hot core and corinos, the column density can vary by about a factor of two. This temperature variation may also affect $\text{CH}_3\text{C}(\text{O})\text{NH}_2$, for which an excitation temperature is determined. The column densities of its ground and first excited vibrational states differ substantially at $(2.2 \pm 1.1) \times 10^{14}$ and $(6 \pm 3) \times 10^{14}$ cm^{-2} , respectively. Due to the large error bar on the determined excitation temperature it is possible that this species is excited at a substantially different temperature. While no other T_{ex} was found for which the column densities of the two states converged, the column densities are consistent within the uncertainties.

For amides for which accurate spectroscopic laboratory data are available, but no convincing lines are found in our observed spectra, upper limits on the column density have been derived. This applies to the following amides (between brackets the line frequency is listed from which the upper limit is calculated): $^{15}\text{NH}_2\text{CHO}$ (233 523.8 MHz), *cis*-NHDCHO

(234 776.2 MHz), $\text{NH}_2\text{CH}^{18}\text{O}$ (231 843.5 and 235 678.6 MHz), $\text{NH}_2\text{C}(\text{O})\text{NH}_2$ (221 615.8 MHz), $\text{NH}_2\text{C}(\text{O})\text{CN}$ (217 621.9 and 218 497.0 MHz), and $\text{HOCH}_2\text{C}(\text{O})\text{NH}_2$ (234 277.2 MHz).

Finally, lines of several oxygen-COMs are also detected. While not the aim of this work, these species are analysed to account for line blending with the amides. Furthermore, some species are of considerable prebiotic interest, such as glycolaldehyde (HOCH_2CHO), the simplest sugar-like molecule. In the SMM1-a spectrum CH_2DOH , acetaldehyde (CH_3CHO), and acetone ($\text{CH}_3\text{C}(\text{O})\text{CH}_3$) are securely identified (see supplementary information Figs. 12, 13, and 14), while acetic acid (CH_3COOH) and HOCH_2CHO are tentatively detected (see supplementary information Figs. 15 and 16).

The number of identified lines and fit parameters of all species are presented in Table 1, while the line parameters of the identified transitions are listed in Table 3 in the supporting information.

Table 1: Best fit parameters for the molecules investigated in this work.

Molecule	Lines #	N_T (cm^{-2})	T_{ex} (K)	V_{LSR} (km s^{-1})	ΔV (km s^{-1})	$[X] / [\text{NH}_2\text{CHO}]^a$	$[X] / [\text{CH}_3\text{OH}]^b$	$[X] / [\text{H}_2]$
$\text{NH}_2^{13}\text{CHO}$	2	$(7.5 \pm 1.2) \times 10^{13}$	[200]	6.8 ± 0.2	2.6 ± 0.4	—	$(7 \pm 3) \times 10^{-5}$	$(8 \pm 4) \times 10^{-11}$
$\text{NH}_2^{12}\text{CHO}^c$	7	$[(3.9 \pm 1.3) \times 10^{15}, c]$	—	—	—	1.0×10^0	$(3.5 \pm 1.7) \times 10^{-3}$	$(3 \pm 2) \times 10^{-9}$
NH_2CHO , $\nu_{12}=1$	3	$(1.0 \pm 0.2) \times 10^{15}$	[200]	6.9 ± 0.1	2.8 ± 0.2	$(2.6 \pm 1.0) \times 10^{-1}$	$(9 \pm 4) \times 10^{-4}$	$(1.0 \pm 0.5) \times 10^{-9}$
NH_2CDO	2	$\sim (1.4 \pm 0.3) \times 10^{14}$	[200]	6.4 ± 0.2	3.0 ± 0.5	$\sim (3.6 \pm 1.4) \times 10^{-2}$	$\sim (1.3 \pm 0.5) \times 10^{-4}$	$\sim (1.4 \pm 0.7) \times 10^{-10}$
trans-NHDCHO	3	$\sim (4.3 \pm 1.6) \times 10^{13}$	[200]	7.4 ± 0.6	3.3 ± 0.4	$\sim (1.1 \pm 0.6) \times 10^{-2}$	$\sim (4 \pm 2) \times 10^{-5}$	$\sim (4 \pm 3) \times 10^{-11}$
$\text{CH}_3\text{C}(\text{O})\text{NH}_2$, $\nu=0$	7	$(2.2 \pm 1.1) \times 10^{14}$	235 ± 80	6.4 ± 0.2	1.5 ± 0.4	$(6 \pm 3) \times 10^{-2}$	$(2.0 \pm 1.2) \times 10^{-4}$	$(2.2 \pm 1.5) \times 10^{-10}$
$\text{CH}_3\text{C}(\text{O})\text{NH}_2$, $\nu=1$	5	$(6 \pm 3) \times 10^{14}$	[235]	6.9 ± 0.5	[1.5]	$(1.4 \pm 1.0) \times 10^{-1}$	$(5 \pm 3) \times 10^{-4}$	$(6 \pm 4) \times 10^{-10}$
CH_3NHCHO , $\nu=0$	1	$\sim (6 \pm 3) \times 10^{14}$	[200]	7.3 ± 0.6	2.3 ± 0.5	$\sim (1.5 \pm 0.9) \times 10^{-1}$	$\sim (6 \pm 3) \times 10^{-4}$	$\sim (6 \pm 4) \times 10^{-10}$
CH_3NHCHO , $\nu=1$	1	$\sim (6 \pm 4) \times 10^{14}$	[200]	7.5 ± 0.8	2.3 ± 0.5	$\sim (1.5 \pm 1.0) \times 10^{-1}$	$\sim (5 \pm 4) \times 10^{-4}$	$\sim (6 \pm 4) \times 10^{-10}$
$^{15}\text{NH}_2\text{CHO}$	0	$\leq 1.5 \times 10^{14}$	[200]	[7.0]	[3.0]	$\leq 3.8 \times 10^{-2}$	$\leq 1.4 \times 10^{-4}$	$\leq 1.5 \times 10^{-10}$
cis-NHDCHO	0	$\leq 1.0 \times 10^{14}$	[200]	[7.0]	[3.0]	$\leq 2.6 \times 10^{-2}$	$\leq 9.1 \times 10^{-5}$	$\leq 1.0 \times 10^{-10}$
$\text{NH}_2\text{CH}^{18}\text{O}$	0	$\leq 1.5 \times 10^{14}$	[200]	[7.0]	[3.0]	$\leq 3.8 \times 10^{-2}$	$\leq 1.4 \times 10^{-4}$	$\leq 1.5 \times 10^{-10}$
$\text{NH}_2\text{C}(\text{O})\text{NH}_2$	0	$\leq 5.0 \times 10^{13}$	[200]	[7.0]	[3.0]	$\leq 1.3 \times 10^{-2}$	$\leq 4.5 \times 10^{-5}$	$\leq 5 \times 10^{-11}$
$\text{NH}_2\text{C}(\text{O})\text{CN}$	0	$\leq 2.0 \times 10^{14}$	[200]	[7.0]	[3.0]	$\leq 5.1 \times 10^{-2}$	$\leq 1.8 \times 10^{-4}$	$\leq 2.0 \times 10^{-10}$
$\text{HOCH}_2\text{C}(\text{O})\text{NH}_2$	0	$\leq 5.0 \times 10^{13}$	[200]	[7.0]	[3.0]	$\leq 1.3 \times 10^{-2}$	$\leq 4.5 \times 10^{-5}$	$\leq 5 \times 10^{-11}$
CH_3OH^b	5	$[1.1 \times 10^{18}]^b$	—	—	—	—	1.0×10^0	$(1.1 \pm 0.3) \times 10^{-6}$
CH_2DOH	4	$(1.2 \pm 0.2) \times 10^{16}$	$[250]^d$	7.5 ± 0.1	2.3 ± 0.2	$(3.1 \pm 1.1) \times 10^0$	$(1.1 \pm 0.4) \times 10^{-2}$	$(1.2 \pm 0.6) \times 10^{-8}$
CH_3CHO	6	$(1.5 \pm 0.2) \times 10^{15}$	170 ± 10	7.8 ± 0.1	3.4 ± 0.2	$(3.8 \pm 1.4) \times 10^{-1}$	$(1.4 \pm 0.5) \times 10^{-3}$	$(1.5 \pm 0.7) \times 10^{-9}$
$\text{CH}_3\text{C}(\text{O})\text{CH}_3$	4	$(8 \pm 3) \times 10^{15}$	250 ± 40	7.4 ± 0.2	3.4 ± 0.3	$(2.1 \pm 1.0) \times 10^0$	$(7 \pm 4) \times 10^{-3}$	$(8 \pm 5) \times 10^{-9}$
CH_3COOH	2	$\sim (2.8 \pm 0.7) \times 10^{15}$	180 ± 40	7.4 ± 0.2	3.6 ± 0.6	$\sim (7 \pm 3) \times 10^{-1}$	$\sim (2.5 \pm 1.1) \times 10^{-3}$	$\sim (2.8 \pm 1.4) \times 10^{-9}$
HOCH_2CHO	4	$\sim (1.6 \pm 0.2) \times 10^{15}$	220 ± 20	6.8 ± 0.3	4.6 ± 0.3	$\sim (4.1 \pm 1.5) \times 10^{-1}$	$\sim (1.5 \pm 0.6) \times 10^{-3}$	$\sim (1.6 \pm 0.7) \times 10^{-9}$
H_2CCO	0	$\leq 1.5 \times 10^{16}$	[200]	[7.0]	[3.0]	$\leq 3.8 \times 10^0$	$\leq 1.4 \times 10^{-2}$	$\leq 1.5 \times 10^{-8}$

Values of T_{ex} , V_{LSR} , and ΔV in square brackets are estimated. The \sim symbol indicates a tentative identification and \leq an upper limit.

^aThe $[X]/[\text{NH}_2\text{CHO}]$ values are determined based on the NH_2CHO column density, which is derived from the column density of the optically thin $\text{NH}_2^{15}\text{CHO}$ isotopologue.

^bThe CH_3OH main isotopologue column density is taken from Ligterink et al.²⁶, which is based on the $\text{CH}_3^{18}\text{OH}$ column density of $(2.0 \pm 1.1) \times 10^{15} \text{ cm}^{-2}$ multiplied by a $^{16}\text{O}/^{18}\text{O}$ ratio of 560^{37} .

^cThe $\text{NH}_2^{12}\text{CHO}$ column density is determined from the $\text{NH}_2^{13}\text{CHO}$ column density, multiplied by a $^{12}\text{C}/^{13}\text{C}$ ratio of 52.5 ± 15.4^{38} . The number of lines listed are those identified of NH_2CHO .

^dThe fit of CH_2DOH makes use of the T_{ex} determined for $\text{CH}_3^{18}\text{OH}$ by Ligterink et al.²⁶.

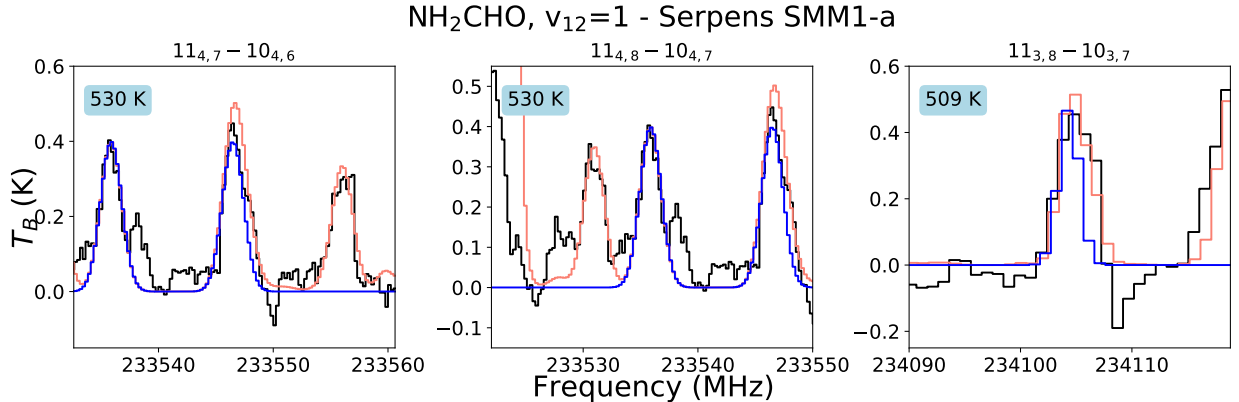


Figure 1: Identified lines of NH₂CHO, $\nu_{12}=1$ toward SMM1-a. The observed spectrum is plotted in black, with the synthetic spectrum of the species overplotted in blue, and the synthetic spectrum of all fitted species combined in red. The transition is indicated at the top of each panel and the upper state energy is given in the top left of each panel. Detected transitions of NH₂CHO $\nu=0$, NH₂¹³CHO, NH₂CDO, and NHDCHO are presented in the supporting information section.

Discussion

The detected molecules presented in Sect. Results substantially expand the number of identified species in Serpens SMM1^{24,26,27}. Particularly noteworthy is the detection of CH₃C(O)NH₂, making SMM1-a the lowest luminosity and mass object where acetamide is securely identified, with only a tentative detection of the molecule in the low-mass protostar IRAS 16293–2422B²⁰. Also, the tentative identification of deuterated formamide and CH₃NHCHO in SMM1-a add constraints to two molecules for which not many detections are found in the literature^{9,12,13,15,19}.

In the following three sections, comparisons are made with the molecular inventories of other extraterrestrial sources. An overview of these sources, including relevant molecular abundances and column densities, is found in the supplementary information Table 4. The list covers a diverse set of objects, such as the comets 67P/Churyumov-Gerasimenko (hereafter 67P/C-G) and 46P/Wirtanen or the giant molecular cloud G+0.693, where the molecular complexity is driven by shocks resulting from a cloud-cloud collision³⁹. Data from

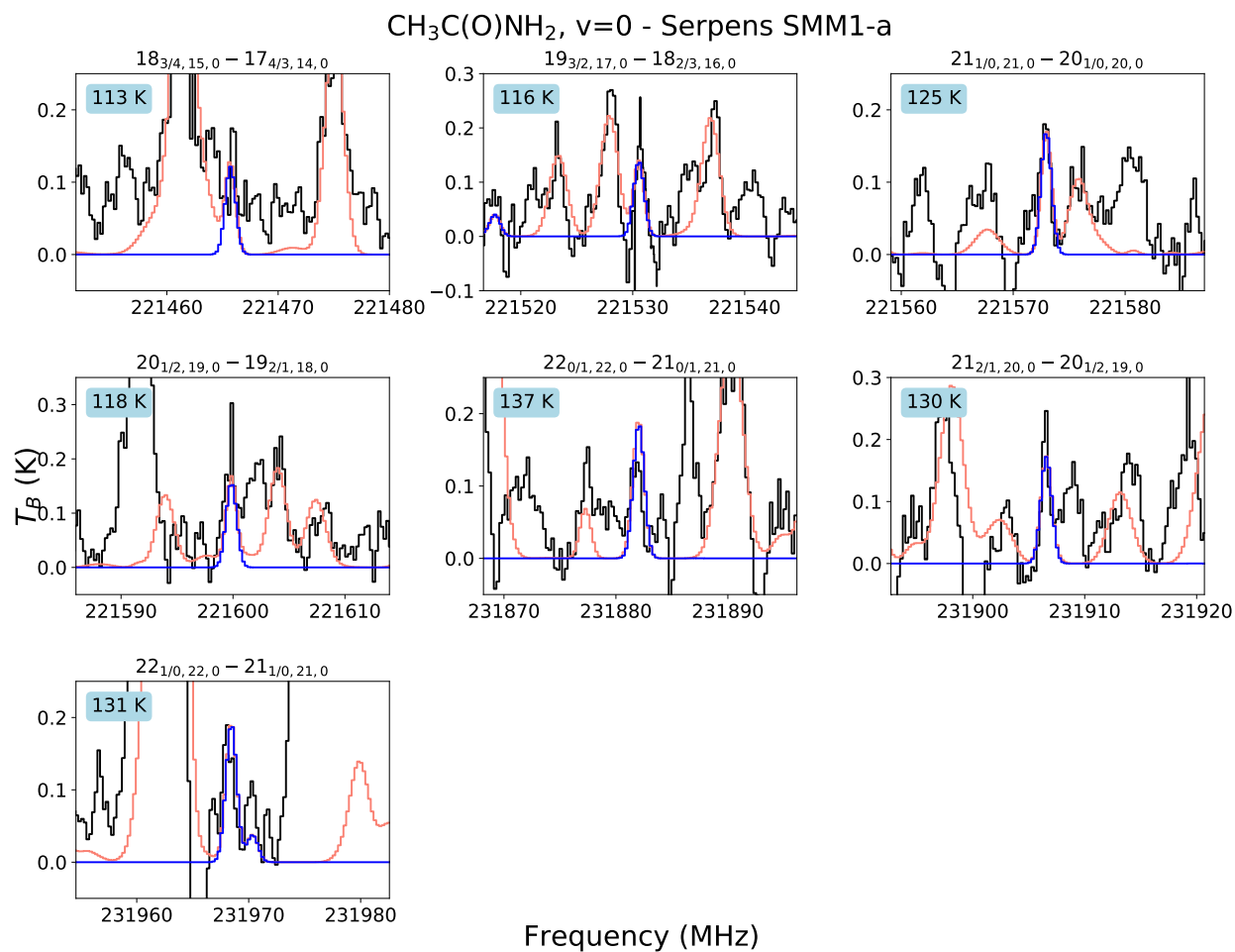


Figure 2: Identified lines of $\text{CH}_3\text{C}(\text{O})\text{NH}_2$, $\nu=0$ toward SMM1-a. The observed spectrum is plotted in black, with the synthetic spectrum of the species overplotted in blue, and the synthetic spectrum of all fitted species combined in red. The transition is indicated at the top of each panel and the upper state energy is given in the top left of each panel. Detected transitions of $\text{CH}_3\text{C}(\text{O})\text{NH}_2$, $\nu=1$ are presented in the supporting information.

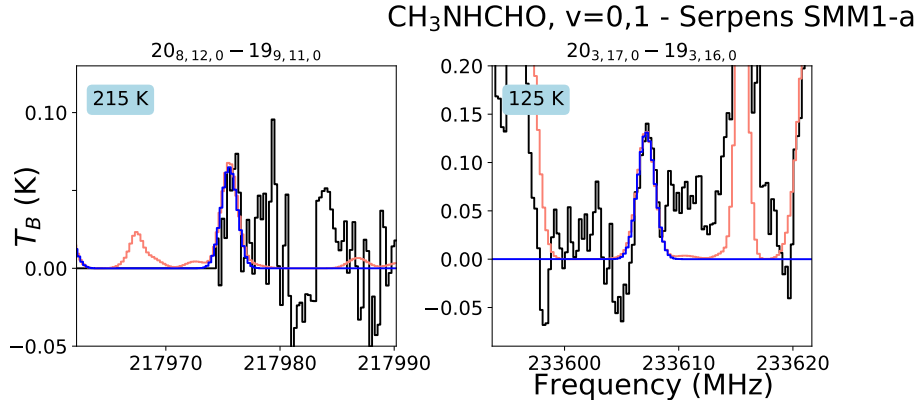


Figure 3: Identified lines of CH₃NHCHO, $\nu=0,1$ toward SMM1-a. The observed spectrum is plotted in black, with the synthetic spectrum of the species overplotted in blue, and the synthetic spectrum of all fitted species combined in red. The transition is indicated at the top of each panel and the upper state energy is given in the top left of each panel.

the low-mass protostars Perseus B1-c (hereafter B1-c), Serpens S68N (hereafter S68N), Per-emb 44, Per-emb 12 B, Per-emb 13, Per-emb 27, Per-emb 29, and IRAS 16293–2422B are used. High-mass protostars and star-forming regions are represented in G328.2551–0.5321 (hereafter G328), W3(H₂O), NGC 6334I, G31.41+0.31, GAL 034.3+00.2, Orion KL, NGC 7538 IRS1, NGC 6334-29, AFGL 4176, GAL 10.47+00.03, G10.6-0.4, and Sagittarius B2 (hereafter Sgr B2). Most of these objects have been observed with interferometric observations, but data for 46P/Wirtanen, G+0.693, W3(H₂O), GAL 034.3+00.2, NGC 7538 IRS1, NGC 6334-29, GAL 31.41+0.31, GAL 10.47+00.03, Sgr B2(M), and Sgr B2(N) has been obtained with a variety of single dish telescopes. Data for 67P/C-G was obtained by the Rosetta space exploration mission.

The NH₂CHO – CH₃C(O)NH₂ link

Since the first detection of acetamide it has been suggested that CH₃C(O)NH₂ forms in reactions starting from NH₂CHO¹¹. If this is the case, a column density correlation between the two species may be observed. In the left side panels of Fig. 5 the results of this study and literature data are collected and the ratios between NH₂CHO and CH₃C(O)NH₂ are presented in a scatter plot and bar graph. Literature data are taken from a variety of

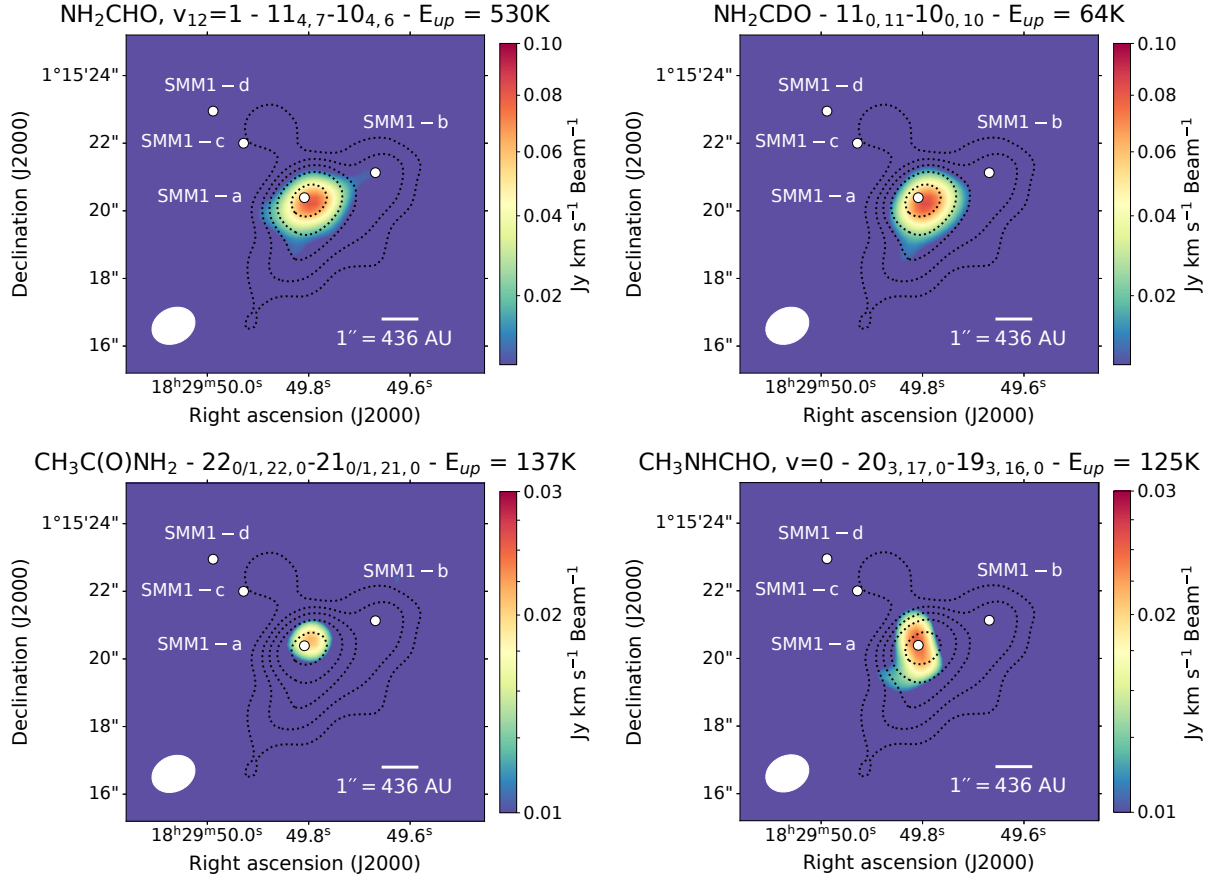


Figure 4: Moment 0 maps of lines of NH_2CHO , $\nu_{12}=1$, NH_2CDO , $\text{CH}_3\text{C}(\text{O})\text{NH}_2$, and CH_3NHCHO toward SMM1. All lines are integrated over eight velocity bins, centred on the peak frequency of each line as determined toward SMM1-a. Positions of protostars in the SMM1 region are indicated and the beam size ($1.32'' \times 1.04''$) is visualised in the bottom left corner. Dust continuum contours are given by the black dotted line at the levels of 0.02, 0.05, 0.1, 0.2, and 0.5 Jy Beam^{-1} .

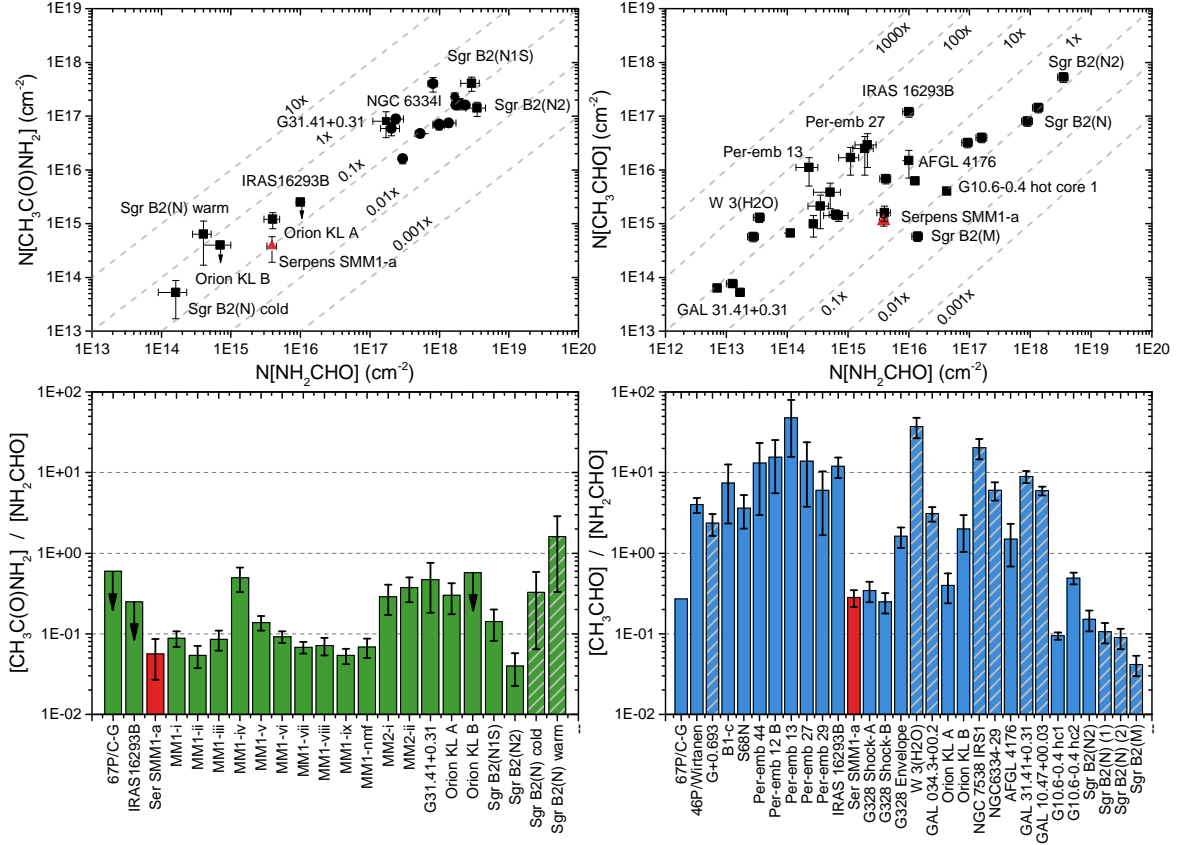


Figure 5: Scatter plots and bar graphs of the $\text{CH}_3\text{C}(\text{O})\text{NH}_2 / \text{NH}_2\text{CHO}$ ratio (left) and $\text{CH}_3\text{CHO} / \text{NH}_2\text{CHO}$ ratio (right) toward various interstellar sources. Serpens SMM1-a is indicated with a red triangle or red bar. For readability the NGC 6334I sources are grouped together and indicated with a circle and abbreviated as MM1-i to MM2-ii. Also for readability, only a select number of sources are labeled in the $\text{CH}_3\text{CHO} / \text{NH}_2\text{CHO}$ scatter plot. The sources in the bar plot are roughly ordered by luminosity. Single dish observations are indicated with striped bars. Column densities taken from the literature^{9,10,12,13,15,16,19,20,40–55} are presented in Table S3 in the supporting information.

sources, ranging from comets to protostars and star-forming regions, with vastly varying luminosities and masses.

From Fig. 5 it becomes apparent that NH_2CHO and $\text{CH}_3\text{C}(\text{O})\text{NH}_2$ column densities strongly correlate. A $\text{CH}_3\text{C}(\text{O})\text{NH}_2 / \text{NH}_2\text{CHO}$ ratio of approximately 0.1 with a scatter of less than an order of magnitude is found, in particular when single dish data are omitted. The correlation is especially prominent when contrasted to $\text{CH}_3\text{CHO} / \text{NH}_2\text{CHO}$ ratios, which easily scatter over 2 to 3 orders of magnitude, see right side panels of Fig. 5. Furthermore,

it is interesting to point out that this ratio is similar in a diverse set of objects with very different physical characteristics, such as luminosity and protostellar mass, as these sources range from the low end of the mass range and low-luminosity, such as IRAS 16293–2422B ($\sim 3L_{\odot}$ ⁵⁶) and Ser SMM1-a ($\sim 100 L_{\odot}$) to complex, multi-protostar, high-mass star-forming regions with luminosities of 1000s or 10000s L_{\odot} (e.g., NGC 6334I, Sgr B2(N)). In line with the conclusions of Colzi et al.¹⁵, derived from a similar set of data, this points to a chemical link between the two species and/or a similar response of reaction pathways to physical conditions⁵⁷. Formation of $\text{CH}_3\text{C}(\text{O})\text{NH}_2$ and NH_2CHO in the ice mantles of grains in dark clouds or during warm-up toward the protostellar stage followed by release to the gas-phase due to thermal desorption is a likely scenario. This is in line with modeling work of Quénard et al.⁵⁷, who find that NH_2CHO production at high temperatures (i.e., in or near a hot core/corino) is primarily the result of desorbing ice mantles. In contrast, the large differences seen in the $\text{CH}_3\text{CHO} / \text{NH}_2\text{CHO}$ ratio, hint at a more complex interplay of reaction pathways and response to physical conditions for one or both of these species. Prominent gas-phase formation pathways are known for CH_3CHO , such as $\text{CH}_3\text{CH}_2 + \text{O} \rightarrow \text{CH}_3\text{CHO} + \text{H}$ ^{58,59}, and its gas-phase formation has been hinted at in other interstellar sources, such as the L1157-B1 shock⁶⁰.

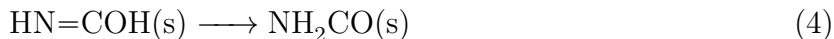
Formation of acetamide by gas-phase reactions and the possible chemical link with formamide have been relatively well investigated, mainly by computational studies^{11,55,61–65}. While solid-state formation of acetamide has been seen in various experiments^{20,66–68}, formation pathways and the chemical link with NH_2CHO are less well established.

Reactions involving the NH_2CO (carbamoyl) radical have been suggested as solid-state pathways to form amides in the literature^{20,69}. One solid-state link between formamide and acetamide is found in the reaction between the methyl and carbamoyl radical:



The carbamoyl radical links acetamide and formamide, since this radical can be formed by abstraction, radiolysis, and photolysis of NH_2CHO , via the $\text{NH}_2 + \text{CO}$ radical addition, via the radical reaction $\text{CN} + \text{H}_2\text{O}$ ⁷⁰, or by hydrogenation of HNCO ⁷¹. Variations on above reaction may be possible, for example by exchanging CH_3 with the methylene (CH_2) radical and an additional hydrogenation step. To further elucidate reactions involving carbamoyl, matrix isolation experiments should be conducted to determine to which extent this and related reactions contribute to the formation of acetamide with formamide.

Another chemical link between formamide and acetamide is found in reactions starting from cyanides. With quantum chemical calculations, Rimola et al.⁷⁰ found a formamide formation pathway starting from the CN radical and water:



There exists an analogue of this reaction for the formation of acetamide, starting from acetonitrile (CH_3CN) and water, which also has been proposed as a gas-phase reaction pathway⁶⁴:



Important to note is that above reactions start with a closed shell species (Eq. 6, while the pathway to form NH_2CHO begins with the CN radical (Eq. 3). However, if the CH_3CN reaction proceeds, this could explain a chemical link between NH_2CHO and $\text{CH}_3\text{C(O)NH}_2$, if there is a relation between $(\text{H})\text{CN}$ and CH_3CN formed in interstellar ices and their abundances are high enough. In the literature, there is some experimental evidence that acetamide

can be formed from CH_3CN . Bulak et al.⁷² investigated the photoprocessing of $\text{CH}_3\text{CN}:\text{H}_2\text{O}$ ice mixtures with laser desorption post-ionization time-of-flight mass spectrometry and identified mass signatures that can be assigned to acetamide. However, an unambiguous identification was not made. Furthermore, Duvernay et al.⁷³ investigated the solid-state formation and photoprocessing of alpha-aminoethanol ($\text{CH}_3\text{C}(\text{OH})\text{NH}_2$) a molecule that shows some chemical similarity to the $\text{CH}_3\text{C}(\text{OH})=\text{NH}$ intermediate produced in reaction 6. Photoprocessing of this species resulted in the formation of acetamide, hinting that reaction 7 may result in the same product.

Several other reactions that form $\text{CH}_3\text{C}(\text{O})\text{NH}_2$ are possible, albeit that none of these show a direct chemical link with NH_2CHO . Among them, the reaction between ketene (H_2CCO) and ammonia (NH_3) is an interesting one that warrants further investigations. The gas-phase reaction of these two molecules has been investigated⁶⁵, but limited experimental evidence for a solid-state equivalent exists. Haupa et al.⁷⁴ investigated the hydrogen abstraction of $\text{CH}_3\text{C}(\text{O})\text{NH}_2$, resulting in the formation of the $\text{CH}_2\text{C}(\text{O})\text{NH}_2$ radical. Photoprocessing of this radical resulted in ketene formation. This can hint that a reverse pathway, starting from H_2CCO may be possible. It is worth noting that only one H_2CCO line is covered in the SMM1-a spectrum, which is not detected, making it difficult to assess ketene as a precursor of acetamide from these observations.

To conclude, observations indicate that the column densities of NH_2CHO and $\text{CH}_3\text{C}(\text{O})\text{NH}_2$ might be correlated. However, the exact nature of this correlation is as of yet unknown and could be due to linked chemical processes, either in the gas-phase or in the solid-state, or production of these species under similar physical conditions.

Deuterated formamide

Lines of two deuterated forms of formamide are tentatively detected in the SMM1-a spectrum, namely trans-NHDCHO and NH_2CDO , see Figs. S4 and S5. While the number of detected lines of these species is insufficient to claim a secure detection, they can be used to

give an indication of D/H fraction of NH_2CHO in SMM1-a and be compared with the values of IRAS 16293–2422B, the only source for which formamide D/H is thoroughly analysed⁹.

Deuterium fractions of $\sim(1.1\pm 0.5)\times 10^{-2}$ and $\sim(3.6\pm 1.0)\times 10^{-2}$ are found for trans-NHDCHO and NH_2CDO , respectively, toward SMM1-a, which agree reasonably well with the $\text{CH}_2\text{DOH} / \text{CH}_3\text{OH}$ ratio of $(1.1\pm 0.4)\times 10^{-2}$. The difference in abundance between trans-NHDCHO and NH_2CDO of a factor of three is peculiar. This can indicate something about the underlying chemistry, but additional observations of deuterated formamide spectral lines are needed to further constrain the synthetic fit and in turn their abundances. Within the error bars, the SMM1 abundances with respect to NH_2CHO match those found toward IRAS 16293–2422, see left panel of Fig. 6. This hints that similar physico-chemical processes are taking place in both sources that result in the formation of formamide and its deuterium isotopomers.

The formation of formamide is still strongly debated, with proponents for gas-phase and solid-state chemistry⁷⁵. Traditionally, deuteration levels of several percent, as found for SMM1-a, are seen as an indication that ice chemistry is producing these species⁷⁶. For formamide, Skouteris et al.⁷⁷ showed that the gas-phase reaction $\text{NH}_2 + \text{H}_2\text{CO} \rightarrow \text{NH}_2\text{CHO} + \text{H}$ can also be efficient in forming deuterated formamide. However, in this scenario, the high deuteration levels of H_2CO and NH_2 (or its precursor) have to be set on the grains. This raises the question whether one set of species can form on grains (H_2CO , NH_2) and the other will not (NH_2CHO), while laboratory evidence shows that both can simultaneously be formed in simulated interstellar ice mantles⁷⁸. Exclusive gas-phase formation of formamide in hot cores seems unlikely.

Other amides

The last couple of years have seen a boost in searches for and detections of amides, especially N-methylformamide and carbamide. In the middle and right panel of Fig. 6 the tentative detection of CH_3NHCHO and upper limit of $\text{NH}_2\text{C}(\text{O})\text{NH}_2$ toward SMM1-a are compared

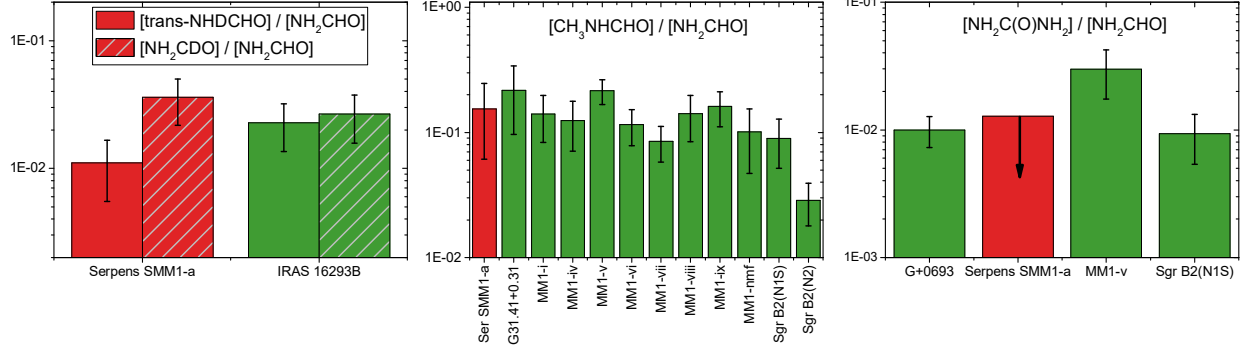


Figure 6: Bar graph plots of deuterated formamide (left), N-methylformamide (middle), and carbamide (right) abundances with respect to NH_2CHO toward SMM1-a (red) and IRAS 16293–2422B⁹, G31.41+0.31¹⁵, NGC 6334I MM1¹⁹, Sgr B2(N)^{12,13}, and G+0.693¹⁶ (all in green). This work and Coutens et al.⁹ use different values for the $^{12}\text{C}/^{13}\text{C}$ ratio^{38,79}. For consistency, the NH_2CHO column density has been determined in both sources with the $^{12}\text{C}/^{13}\text{C} = 52.5 \pm 15.4$ ³⁸ ratio in order to compare the formamide D/H ratios. For readability the NGC 6334I sources MM1-i to MM1-nmf are listed by their abbreviated names. The SMM1-a detection of deuterated NH_2CHO and CH_3NHCHO are tentative, while $\text{NH}_2\text{C}(\text{O})\text{NH}_2$ is not detected and an upper limit is derived. The literature data used in this figure are presented in the supporting information Table S3.

with interstellar detections of these molecules available from the literature.

The $\text{CH}_3\text{NHCHO} / \text{NH}_2\text{CHO}$ ratio in SMM1-a matches with those found in the high-mass sources G31.41+0.31¹⁵, NGC 6334I¹⁹, and Sgr B2(N1S)¹³. This supports the idea that the underlying physico-chemical processes that result in CH_3NHCHO formation in SMM1-a are similar to those in the high-mass objects.

In ice mantles, several CH_3NHCO formation pathways are available^{12,80}, such as the radical-radical addition reactions



and



and the hydrogenation reaction



The tentative correlation between CH_3NHCHO and NH_2CHO can hint that the formation of these two species is linked and that reaction 9 is involved in its formation. It would be of interest to determine the $\text{CH}_3\text{NHCO}/\text{NH}_2\text{CHO}$ toward the giant molecular cloud G+0.693 to see if this correlation also holds at an early stage of star formation. At the same time, parallel detections of CH_3NCO and CH_3NH_2 , of which currently a limited number exist in the literature, may provide insight into the other two formation pathways.

Of the amides that are not detected in SMM1-a, the upper limit abundance of $\text{NH}_2\text{C(O)NH}_2$ can be compared with detections of this molecule in G+0.693 and Sgr B2(N1S) and a tentative identification in NGC 6334I MM1-v^{13,16,19}, see right panel of Fig. 6. The upper limit abundances are found to be similar to those of the detections. This suggests that a slightly deeper search that targets prominent spectral lines of $\text{NH}_2\text{C(O)NH}_2$ may result in a detection of this molecule toward SMM1-a.

Two other complex amides that are searched for in SMM1-a, $\text{NH}_2\text{C(O)CN}$ and $\text{HOCH}_2\text{C(O)NH}_2$, are not detected and at present they have not been detected toward other sources either^{15,17}. The $\text{NH}_2\text{C(O)CN} / \text{NH}_2\text{CHO}$ upper limit ratios are similar in SMM1-a and G31.41+0.31 at ≤ 0.05 and ≤ 0.02 ¹⁵, respectively. For $\text{HOCH}_2\text{C(O)NH}_2$ the upper limits toward SMM1-a, G31.41+0.31, and Sgr B2(N2) are ≤ 0.01 , ≤ 0.004 ¹⁵, and ≤ 0.007 ¹⁷, respectively, with respect to NH_2CHO . Compared to the abundances of $\text{CH}_3\text{C(O)NH}_2$ and CH_3NHCHO with respect to NH_2CHO , which are approximately 0.1, this shows that $\text{NH}_2\text{C(O)CN}$ and $\text{HOCH}_2\text{C(O)NH}_2$ are substantially less abundant by at least a factor 5–25.

It is interesting to note that $\text{NH}_2\text{C(O)CN}$ and $\text{HOCH}_2\text{C(O)NH}_2$ are much less abundant, while their chemical complexity seems to be similar or marginally greater than that of $\text{CH}_3\text{C(O)NH}_2$ and CH_3NHCHO . This suggests that reactions forming these molecules are

substantially less efficient than the pathway(s) leading to $\text{CH}_3\text{C}(\text{O})\text{NH}_2$ and CH_3NHCHO or that these molecules are much more readily destroyed.

Prebiotic chemistry & planetary exploration

The results of this study suggest that SMM1-a has a rich inventory of amides, which have been primarily formed in the ice mantles of interstellar grains and are sublimated in the hot corino. Recent studies indicate that ice formed in the dark cloud is inherited into the planet-forming disk⁸¹. Chemical inventories, including NH_2CHO , of several hot corinos have indeed been shown to be similar to the composition of comet 67P/Churyumov–Gerasimenko^{82,83}. If amides are formed in the dark cloud or during the onset of the protostellar stage, when ice mantles warm up, they can survive into the planet-forming disk and be available as planet building material. Remnants of planet building, such as comets and asteroids, can bombard newly formed planets and seed it with a cocktail of prebiotic molecules, including amides⁸⁴.

More studies of comets and asteroids are needed to determine the amount of amides that are present in these objects. Radio telescope observations may help with this by analyzing the coma gas¹⁰, but observational tools are generally not sensitive enough to detect larger amides, since they are usually less abundant and not very volatile. Space exploration missions are required to explore these chemical inventories in situ, for example with the ORganics Information Gathering Instrument (ORIGIN)¹⁴ space instrument, which is intended to detect large non-volatile prebiotic molecules and biomolecules.

Conclusions

In this publication the amide inventory of the hot corino around the intermediate-mass protostar Serpens SMM1-a is studied. The first detections of NH_2CHO $\nu=0$, NH_2CHO $\nu_{12}=1$, $\text{NH}_2^{13}\text{CHO}$, and $\text{CH}_3\text{C}(\text{O})\text{NH}_2$ $\nu=0,1$ toward this source are presented, as are the tentative identifications of *trans*-NHDCHO, NH_2CDO , and CH_3NHCHO $\nu=0,1$. Serendipitous detec-

tions of the oxygen COMs CH_3CHO and $\text{CH}_3\text{C}(\text{O})\text{CH}_3$ are made, while CH_3COOH and HOCH_2CHO are tentatively identified. Ratios of the detected molecules are derived with respect to NH_2CHO and compared with molecular inventories of a varied sample of other sources.

For $\text{CH}_3\text{C}(\text{O})\text{NH}_2$ and CH_3NHCHO a ratio of approximately 0.1 and a scatter of less than an order of magnitude is found. For $\text{CH}_3\text{C}(\text{O})\text{NH}_2$, for which a larger sample of detections is available, this uniform ratio suggests that there is a link in the formation of this molecule and NH_2CHO and that the ratio must already be set at an early stage of star formation, presumably in ice mantles on dust grains that are present in dark clouds. The D/H ratio of NH_2CHO is found to be about 1–3% and is similar to the ratio derived for IRAS 16293-2422B. This is a strong clue that ice mantle reactions are involved in the formation of NH_2CHO , but further studies are required to assess the extent to which gas-phase reactions are involved. A comparison of the upper limit abundance derived for $\text{NH}_2\text{C}(\text{O})\text{NH}_2$ toward Serpens SMM1-a with those in other sources, suggests that this is a suitable source for follow-up searches for this relevant prebiotic molecule.

The rich amide inventory of Serpens SMM1-a is further evidence for the widespread availability of these molecules in star-forming regions. This increases the likelihood that of these molecules are inherited into comets and other planetesimals and subsequently delivered to planetary surfaces, where they can aid the formation of biomolecules.

Acknowledgement

The authors thank E.G. Bøgelund and E.F. van Dishoeck for valuable discussions of data presented in this manuscript. The authors acknowledge assistance from Allegro, the European ALMA Regional Center node in the Netherlands. We thank the three anonymous reviewers for their helpful comments and suggestions. This paper makes use of the following ALMA data: ADS/JAO.ALMA#2018.1.00836.S. ALMA is a partnership of ESO (represent-

ing its member states), NSF (USA) and NINS (Japan), together with NRC (Canada), MOST and ASIAA (Taiwan), and KASI (Republic of Korea), in cooperation with the Republic of Chile. The Joint ALMA Observatory is operated by ESO, AUI/NRAO and NAOJ. NFWL is supported by the Swiss National Science Foundation (SNSF) Ambizione grant 193453. JKJ is supported by the European Research Council (ERC) under the European Union’s Horizon 2020 research and innovation programme through ERC Consolidator Grant “S4F” (grant agreement No 646908). AC received financial support from the Agence Nationale de la Recherche (grant ANR-19-ERC7-0001-01) and from the European Research Council (ERC) under the European Union’s Horizon 2020 research and innovation programme through the ERC starting grant Chemtrip (grant agreement 949278).

Supporting Information Available

Spectroscopy

Spectroscopic linelists used in the work are primarily taken from the CDMS database, but several linelists from the JPL spectroscopic database and literature sources are used as well. Table 2 gives an overview of the catalogues and identifiers for each molecule analyzed in this work and the main works these entries are based on.

Observed lines

Table 2: References of molecular spectroscopy used in this work

Molecule	ID & Catalogue	Literature
CH ₂ DOH	33004 (JPL)	85–90
H ₂ CCO	42501 (CDMS)	91–93
CH ₃ CHO	44003 (JPL)	94
NH ₂ CHO, $\nu=0$	45512 (CDMS)	95–102
NH ₂ CHO, $\nu_{12}=1$	45516 (CDMS)	95,96,98,99,101
NH ₂ ¹³ CHO	46512 (CDMS)	95–97,100
NH ₂ CDO	46520 (CDMS)	103
cis-NHDCHO	46521 (CDMS)	103
trans-NHDCHO	46522 (CDMS)	103
CH ₃ C(O)CH ₃	58003 (JPL)	104–107
CH ₃ C(O)NH ₂	Literature	108
CH ₃ NHCHO	Literature	12
CH ₃ COOH	60523 (CDMS)	109
HOCH ₂ CHO	60501 (CDMS)	Müller et al. in prep.
NH ₂ C(O)NH ₂	60517 (CDMS)	110–113
NH ₂ C(O)CN	70504 (CDMS)	114,115
HOCH ₂ C(O)NH ₂	75517 (CDMS)	17

Table 3: Spectral information of molecules detected toward SMM1-a

Molecule	Transition $J, K_a, K_c, (F_1, F)$	Frequency (MHz)	E_{up} (K)	A_{ij} (s^{-1})	Minor blending
CH ₂ DOH	10 1 10 0 - 9 0 9 1	221 391.766 (0.0101)	120	2.85×10^{-5}	-
	10 1 9 0 - 9 2 8 0	231 840.297 (0.0097)	124	1.66×10^{-5}	CH ₃ ¹⁸ OH
	9 2 7 0 - 9 1 8 0	231 969.226 (0.0101)	113	8.64×10^{-5}	CH ₃ CHO
	8 2 6 0 - 8 1 7 0	234 471.033 (0.0098)	94	8.43×10^{-5}	-
H ₂ CCO ^a	11 8 3 - 10 8 2	221 546.0454 (0.0225)	895	5.77×10^{-5}	-
	11 8 4 - 10 8 3	221 546.0454 (0.0225)	895	5.77×10^{-5}	-
CH ₃ CHO	12 3 10 1 - 11 3 9 1	231 748.7186 (0.0036)	93	3.94×10^{-4}	CH ₃ OCHO
	12 3 9 2 - 11 3 8 2	231 847.5795 (0.0037)	93	3.94×10^{-4}	CH ₃ OCHO
	12 2 10 2 - 11 2 9 2	234 795.4555 (0.0039)	82	4.28×10^{-4}	CH ₃ OCHO (w)
	12 2 10 0 - 11 2 9 0	234 825.8718 (0.0039)	82	4.28×10^{-4}	-
	12 2 10 3 - 11 2 9 3	234 902.9702 (0.0096)	287	4.31×10^{-4}	-
	12 1 11 3 - 11 1 10 3	235 217.8542 (0.0087)	282	4.43×10^{-4}	-
NH ₂ CHO, $\nu=0$	10 1 9 - 9 1 8	218 459.213 (0.0100)	61	7.48×10^{-4}	-
	11 8 3 - 10 8 2	233 488.887 (0.0009)	258	4.36×10^{-4}	CH ₃ OCHO
	11 8 4 - 10 8 3	233 488.887 (0.0009)	258	4.36×10^{-4}	CH ₃ OCHO

Continued on next page

Table 3 – Continued from previous page

Molecule	Transition $J, K_a, K_c, (F_1, F)$	Frequency (MHz)	E_{up} (K)	A_{ij} (s^{-1})	Minor blending species
	11 9 2 – 10 9 1	233 492.678 (0.0010)	308	3.06×10^{-4}	–
	11 9 3 – 10 9 2	233 492.678 (0.0010)	308	3.06×10^{-4}	–
	11 7 4 – 10 7 3	233 498.065 (0.0100)	213	5.51×10^{-4}	–
	11 7 5 – 10 7 4	233 498.065 (0.0100)	213	5.51×10^{-4}	–
	11 6 6 – 10 6 5	233 527.795 (0.0100)	174	6.51×10^{-4}	CH ₃ CHO (w)
	11 6 5 – 10 6 4	233 527.795 (0.0100)	174	6.51×10^{-4}	CH ₃ CHO (w)
	11 5 7 – 10 5 6	233 594.501 (0.0100)	142	7.36×10^{-4}	–
	11 5 6 – 10 5 5	233 594.501 (0.0100)	142	7.36×10^{-4}	–
	11 3 8 – 10 3 7	234 315.498 (0.0100)	94	8.67×10^{-4}	–
NH ₂ CHO, $\nu_{12}=1$	11 4 7 – 10 4 6	233 551.991 (0.01)	530	8.05×10^{-4}	CH ₃ OCHO (w)
	11 4 8 – 10 4 7	233 541.38 (0.0100)	530	8.05×10^{-4}	–
	11 3 8 – 10 3 7	234 110.228 (0.0100)	509	8.64×10^{-4}	CH ₃ OCHO
NH ₂ ¹³ CHO	11 2 10 – 10 2 9	231 844.16 (0.0022)	79	8.77×10^{-4}	–
	11 3 9 – 10 3 8	233 568.296 (0.0022)	93	8.58×10^{-4}	–
NH ₂ CDO	11 0 11 – 10 0 10	218 022.107 (0.0013)	64	7.49×10^{-4}	–
	12 1 12 – 11 1 11	234 414.679 (0.0013)	76	9.33×10^{-4}	CH ₃ C(O)NH ₂

Continued on next page

Table 3 – Continued from previous page

Molecule	Transition $J, K_a, K_c, (F_1, F)$	Frequency (MHz)	E_{up} (K)	A_{ij} (s^{-1})	Minor blending species
	11 1 10 – 10 1 9	235 136.546 (0.0012)	70	9.35×10^{-4}	CH_3OCHO
cis-NHDCHO ^a	12 0 12 – 11 0 11	234 776.217 (0.0014)	74	9.40×10^{-4}	–
trans-NHDCHO	12 2 11 – 11 2 10	234 250.932 (0.0015)	85	9.12×10^{-4}	–
	12 4 8 – 11 4 7	235 718.042 (0.0014)	121	8.50×10^{-4}	–
	12 3 10 – 11 3 9	235 859.775 (0.0014)	100	8.98×10^{-4}	$\text{CH}_3\text{C}(\text{O})\text{NH}_2$
¹⁵ NH ₂ CHO ^a	11 1 10 – 10 1 9	233 523.780 (0.0032)	70	9.18×10^{-4}	–
NH ₂ CH ¹⁸ O ^a	12 1 12 – 11 1 11	231 843.462 (0.0034)	76	9.03×10^{-4}	–
	12 0 12 – 11 0 11	235 678.570 (0.0035)	74	9.53×10^{-4}	–
CH ₃ C(O)CH ₃	20 2 18 1 – 19 3 17 1	218091.4115 (0.0138)	119	4.31×10^{-4}	–
	20 3 18 1 – 19 2 17 1	218 091.4115 (0.0138)	119	4.31×10^{-4}	–
	19 5 14 0 – 18 6 13 1	234 491.3021 (0.0103)	128	4.15×10^{-4}	–
	19 6 14 0 – 18 7 13 1	234 491.3021 (0.0103)	128	4.15×10^{-4}	–
	20 4 16 1 – 19 5 15 1	235 490.7336 (0.0135)	133	4.68×10^{-4}	trans-NHDCHO, CH ₃ NHCHO, NH ₂ ¹³ CHO
	20 5 16 1 – 19 6 15 1	235 490.7336 (0.0135)	133	4.68×10^{-4}	trans-NHDCHO, CH ₃ NHCHO, NH ₂ ¹³ CHO
	20 4 16 0 – 19 5 15 1	235 548.3327 (0.0107)	133	4.69×10^{-4}	CH ₃ NHCHO

Continued on next page

Table 3 – Continued from previous page

Molecule	Transition $J, K_a, K_c, (F_1, F)$	Frequency (MHz)	E_{up} (K)	A_{ij} (s^{-1})	Minor
	20 5 16 0 – 19 6 15 1	235 548.3327 (0.0107)	133	4.69×10^{-4}	CH ₃ NHCHO
CH ₃ C(O)NH ₂ , $\nu=0$	18 3 15 0 – 17 4 14 0	221 470.562 (0.016)	113	6.01×10^{-4}	–
	18 4 15 0 – 17 3 14 0	221 470.562 (0.016)	113	6.01×10^{-4}	–
	19 3 17 0 – 18 2 16 0	221 535.395 (0.0194)	116	6.14×10^{-4}	–
	19 2 17 0 – 18 3 16 0	221 535.395 (0.0194)	116	6.14×10^{-4}	–
	21 1 21 0 – 20 1 20 0	221 577.81 (0.0291)	125	8.03×10^{-4}	–
	21 0 21 0 – 20 0 20 0	221 577.81 (0.0291)	125	8.03×10^{-4}	–
	20 1 19 0 – 19 2 18 0	221 604.702 (0.0236)	118	2.22×10^{-4}	–
	20 2 19 0 – 19 1 18 0	221 604.702 (0.0236)	118	2.22×10^{-4}	–
	20 1 19 0 – 19 1 18 0	221 604.702 (0.0236)	118	5.39×10^{-4}	–
	20 2 19 0 – 19 2 18 0	221 604.702 (0.0236)	118	5.39×10^{-4}	–
	22 0 22 0 – 21 0 21 0	231 887.118 (0.0341)	137	4.32×10^{-4}	–
	22 1 22 0 – 21 1 21 0	231 887.118 (0.0341)	137	4.32×10^{-4}	–
	22 1 22 0 – 21 0 21 0	231 887.118 (0.0341)	137	5.01×10^{-4}	–
	22 0 22 0 – 21 1 21 0	231 887.118 (0.0341)	137	5.01×10^{-4}	–
	21 2 20 0 – 20 1 19 0	231 911.642 (0.0278)	130	8.52×10^{-4}	–

Continued on next page

Table 3 – Continued from previous page

Molecule	Transition $J, K_a, K_c, (F_1, F)$	Frequency (MHz)	E_{up} (K)	A_{ij} (s^{-1})	Minor blending species
	21 1 20 0 – 20 2 19 0	231 911.642 (0.0278)	130	8.52×10^{-4}	–
	22 1 22 0 – 21 1 21 0	231 973.521 (0.0336)	131	1.24×10^{-4}	–
	22 0 22 0 – 21 0 21 0	231 973.521 (0.0336)	131	1.24×10^{-4}	–
	22 0 22 0 – 21 1 21 0	231 973.521 (0.0336)	131	8.11×10^{-4}	–
	22 1 22 0 – 21 0 21 0	231 973.521 (0.0336)	131	8.11×10^{-4}	–
	22 1 22 0 – 21 1 21 0	231 973.521 (0.0336)	131	8.11×10^{-4}	–
$\text{CH}_3\text{C}(\text{O})\text{NH}_2, \nu=1$	16 7 9 1 – 15 8 8 1	217 631.256 (0.0129)	162	4.43×10^{-4}	–
	18 2 16 1 – 17 3 15 1	217 680.653 (0.0141)	142	3.95×10^{-4}	HOCH_2CN
	18 3 16 1 – 17 3 15 1	217 680.674 (0.0141)	142	2.15×10^{-4}	HOCH_2CN
	18 2 16 1 – 17 2 15 1	217 686.753 (0.0141)	142	2.15×10^{-4}	HOCH_2CN
	18 3 16 1 – 17 2 15 1	217 686.774 (0.0141)	142	3.95×10^{-4}	HOCH_2CN
	17 6 11 1 – 16 7 10 1	221 315.706 (0.0160)	168	5.39×10^{-4}	$\text{CH}_3\text{C}(\text{O})\text{CH}_3$
	9 8 1 1 – 8 7 1 1	231 882.736 (0.0044)	93	5.40×10^{-4}	–
	22 1 21 1 – 21 2 20 1	233 621.037 (0.0318)	197	9.04×10^{-4}	–
	22 2 21 1 – 21 2 20 1	233 621.037 (0.0318)	197	9.04×10^{-4}	–
	20 3 17 0 – 19 3 16 0	233 612.959 (0.0015)	125	5.65×10^{-4}	–
$\text{CH}_3\text{NHCHO}, \nu=0$					

Continued on next page

Table 3 – Continued from previous page

Molecule	Transition $J, K_a, K_c, (F_1, F)$	Frequency (MHz)	E_{up} (K)	A_{ij} (s^{-1})	Minor blending species
$\text{CH}_3\text{NHCHO}, \nu=1$	20 8 12 0 – 19 9 11 0	217 981.125 (0.0021)	215	4.15×10^{-4}	–
$\text{NH}_2\text{C(O)NH}_2^a$	16 4 12 – 15 5 11	221 615.758 (0.05)	104	6.41×10^{-4}	–
	16 5 12 – 15 4 11	221 615.739 (0.0113)	104	6.41×10^{-4}	–
HOCH_2CHO	9 5 5 – 8 4 4	217626.0610 (0.1200)	40	1.59×10^{-4}	–
	25 10 16 – 25 9 17	234765.736 (0.1200)	242	2.04×10^{-4}	$\text{CH}_2\text{DOH (w)}$
	42 9 34 – 42 8 35	235311.3660 (0.1200)	558	2.29×10^{-4}	–
	24 10 15 – 24 9 16	235697.8890 (0.1200)	228	2.03×10^{-4}	CH_3OCHO
CH_3COOH	20 0 20 0 0 – 19 0 19 0 0	218010.0224 (0.0018)	113	7.03×10^{-5}	–
	20 1 20 0 0 – 19 1 19 0 0	218 010.0224 (0.0018)	113	7.03×10^{-5}	–
	20 0 20 0 0 – 19 1 19 0 0	218 010.0224 (0.0018)	113	7.03×10^{-5}	–
	20 1 20 0 0 – 19 0 19 0 0	218 010.0224 (0.0018)	113	7.03×10^{-5}	–
	20 0 20 0 1 – 19 0 19 0 2	218 044.2146 (0.0017)	112	4.50×10^{-5}	CH_3NCO
	20 1 20 0 1 – 19 1 19 0 2	218 044.2146 (0.0017)	112	4.50×10^{-5}	CH_3NCO
	20 0 20 0 1 – 19 1 19 0 2	218 044.2146 (0.0017)	112	4.50×10^{-5}	CH_3NCO
	20 1 20 0 1 – 19 0 19 0 2	218 044.2146 (0.0017)	112	4.50×10^{-5}	CH_3NCO
$\text{NH}_2\text{C(O)CN}^a$	67 18 50 – 67 17 51	217 621.387 (0.1500)	946	4.52×10^{-4}	–

Continued on next page

Table 3 – Continued from previous page

Molecule	Transition $J, K_a, K_c, (F_1, F)$	Frequency (MHz)	E_{up} (K)	A_{ij} (s^{-1})	Minor blending species
	29 15 14 – 29 14 15	217 621.351 (0.0076)	238	3.06×10^{-4}	–
	12 9 4 – 11 8 3	218 496.949 (0.0094)	57	4.81×10^{-4}	–
	12 9 3 – 11 8 4	218 496.953 (0.0094)	57	4.81×10^{-4}	–
	29 6 24 – 28 5 23	218 930.010 (0.1500)	170	3.11×10^{-4}	–
HOCH ₂ C(O)NH ₂ ^a	38 1 37 – 37 1 36	234 277.191 (0.0500)	227	6.12×10^{-4}	–
	38 1 37 – 37 2 36	234 277.191 (0.0500)	227	7.19×10^{-4}	–
	38 2 37 – 37 2 36	234 277.191 (0.0500)	227	6.12×10^{-4}	–
	38 2 37 – 37 1 36	234 277.191 (0.0500)	227	7.19×10^{-4}	–

^aOf undetected species the listed lines are used to determine their upper limit column density.

Line fits

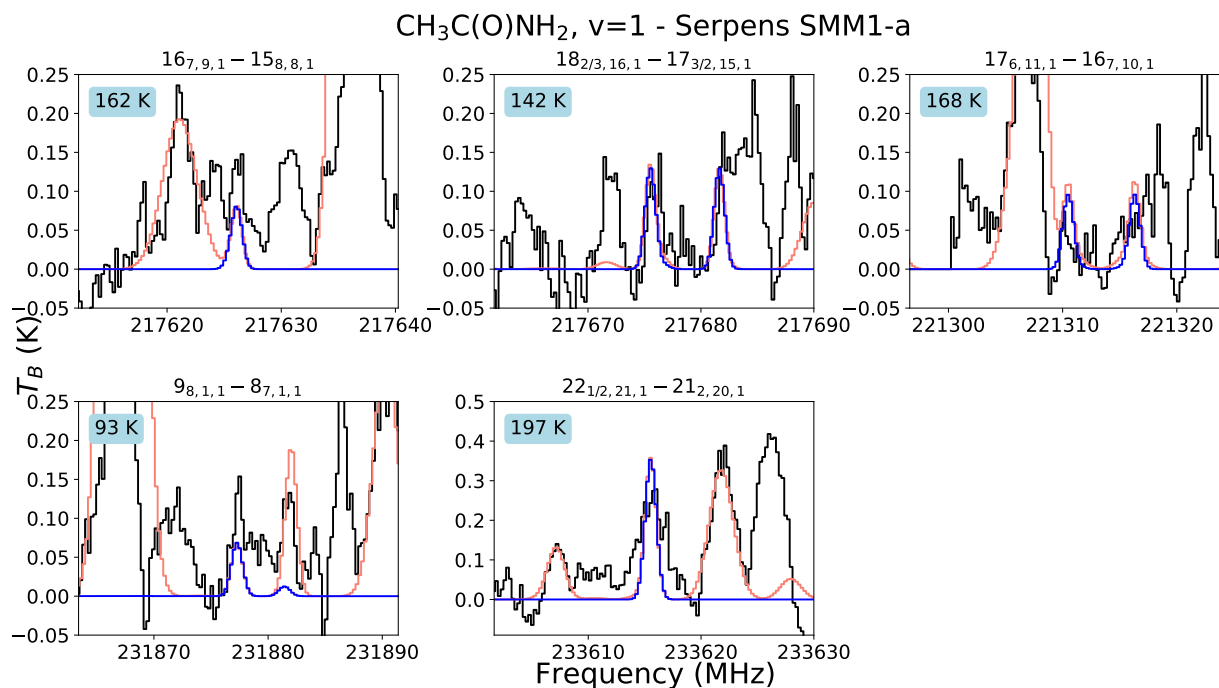


Figure 7: Identified lines of $\text{CH}_3\text{C}(\text{O})\text{NH}_2$, $\nu=1$ toward SMM1-a. The observed spectrum is plotted in black, with the synthetic spectrum of the species overplotted in blue, and the synthetic spectrum of all fitted species combined in red. The transition is indicated at the top of each panel and the upper state energy is given in the top left of each panel.

Literature data

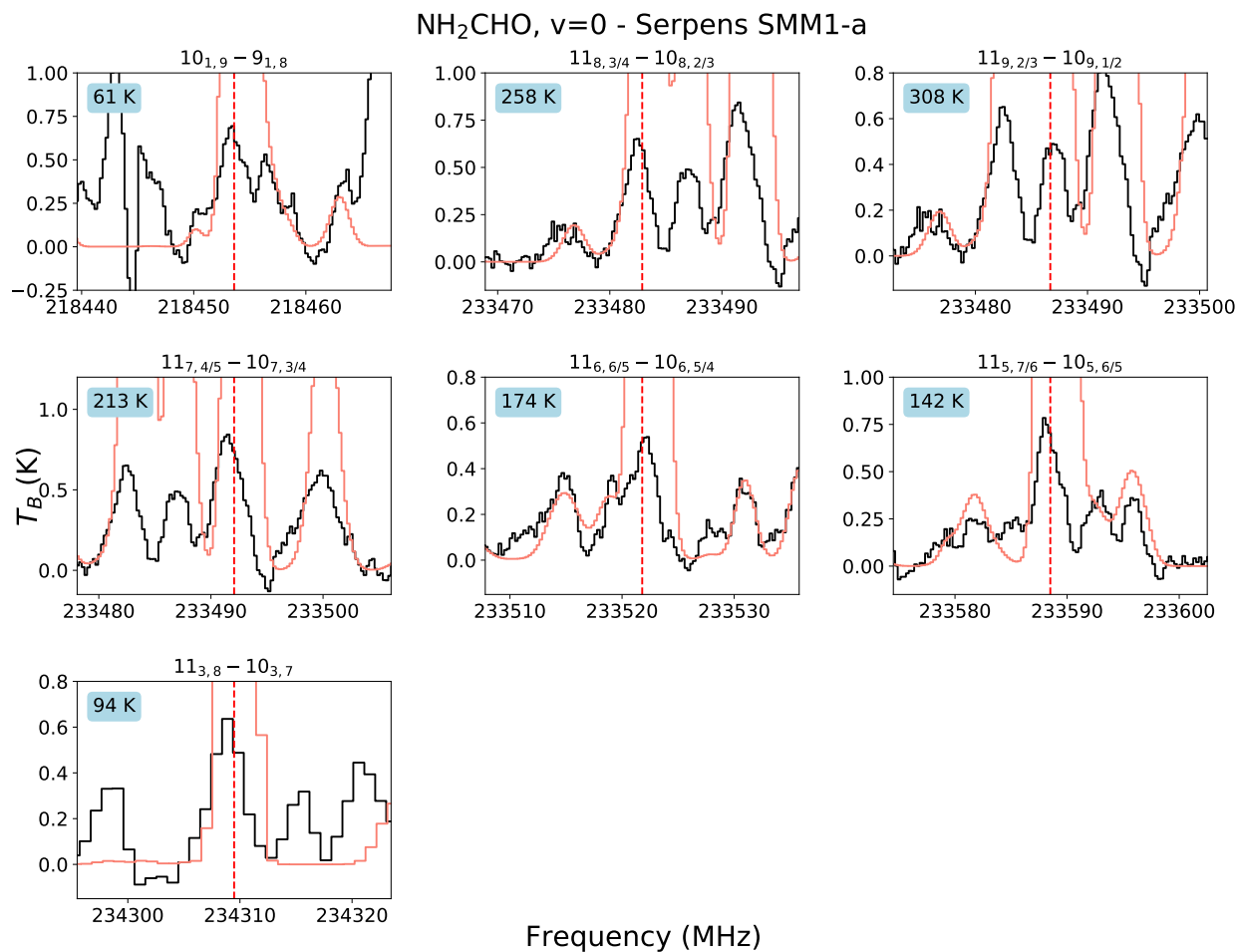


Figure 8: Identified lines of $\text{NH}_2\text{CHO}, \nu=0$ toward SMM1-a. The observed spectrum is plotted in black and the spectral line is indicated with a red dashed line. Since these transitions are optically thick, no synthetic fit of the transition is made. However, the combined synthetic spectrum (red) does show the NH_2CHO spectral lines, which are determined from optically thin $\text{NH}_2^{13}\text{CHO}$ measurements. The transition is indicated at the top of each panel and the upper state energy is given in the top left of each panel.

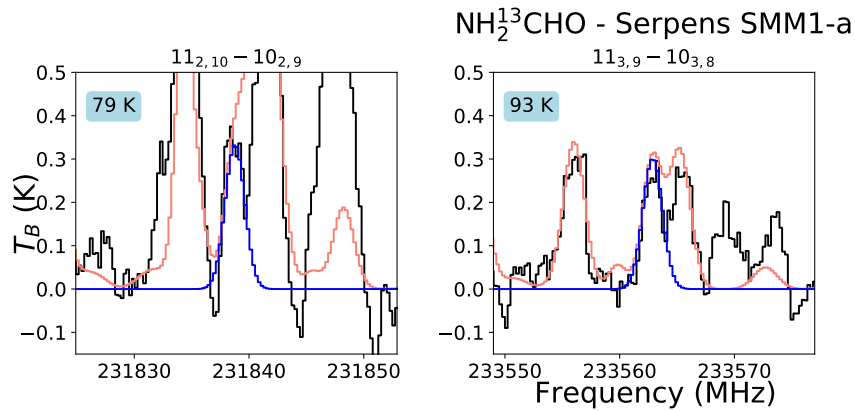


Figure 9: Identified lines of $\text{NH}_2^{13}\text{CHO}$ toward SMM1-a. The observed spectrum is plotted in black, with the synthetic spectrum of the species overplotted in blue, and the synthetic spectrum of all fitted species combined in red. The transition is indicated at the top of each panel and the upper state energy is given in the top left of each panel.

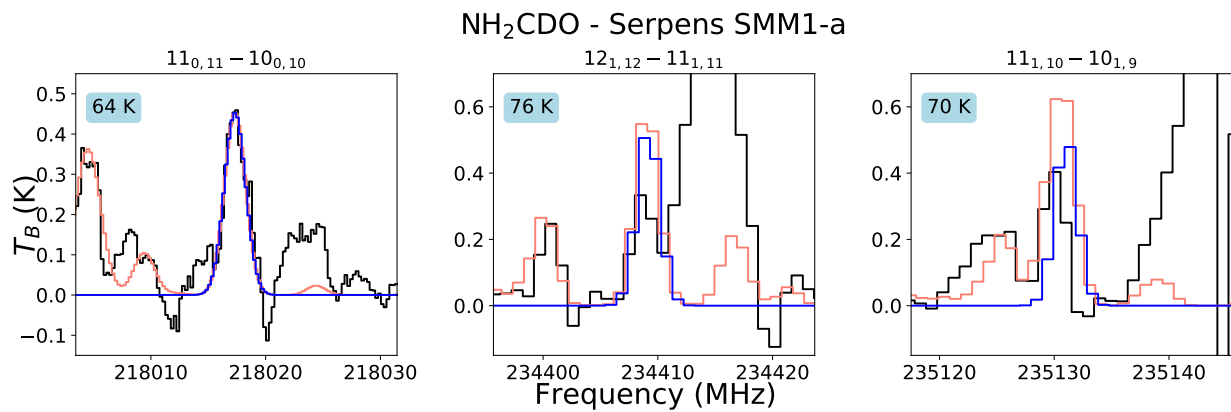


Figure 10: Identified lines of NH_2CDO toward SMM1-a. The observed spectrum is plotted in black, with the synthetic spectrum of the species overplotted in blue, and the synthetic spectrum of all fitted species combined in red. The transition is indicated at the top of each panel and the upper state energy is given in the top left of each panel.

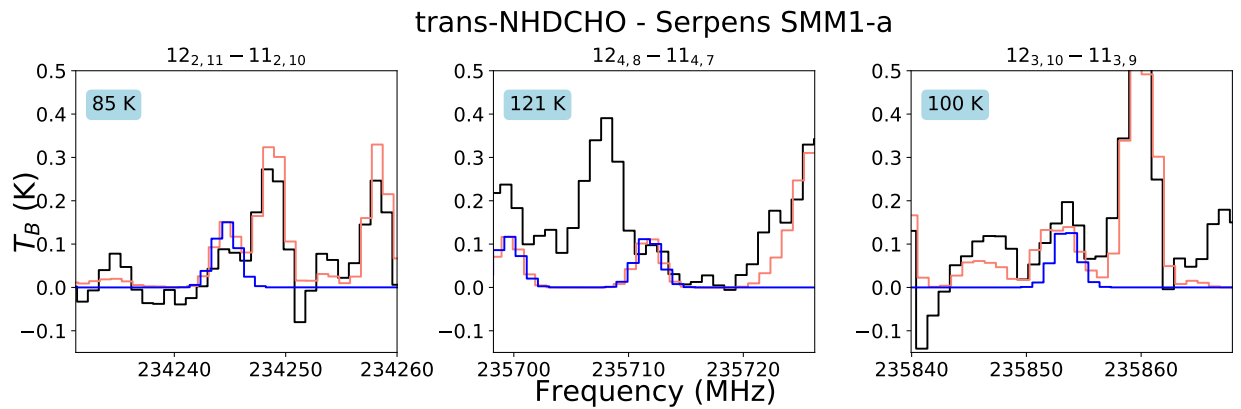


Figure 11: Identified lines of trans-NHDCHO toward SMM1-a. The observed spectrum is plotted in black, with the synthetic spectrum of the species overplotted in blue, and the synthetic spectrum of all fitted species combined in red. The transition is indicated at the top of each panel and the upper state energy is given in the top left of each panel.

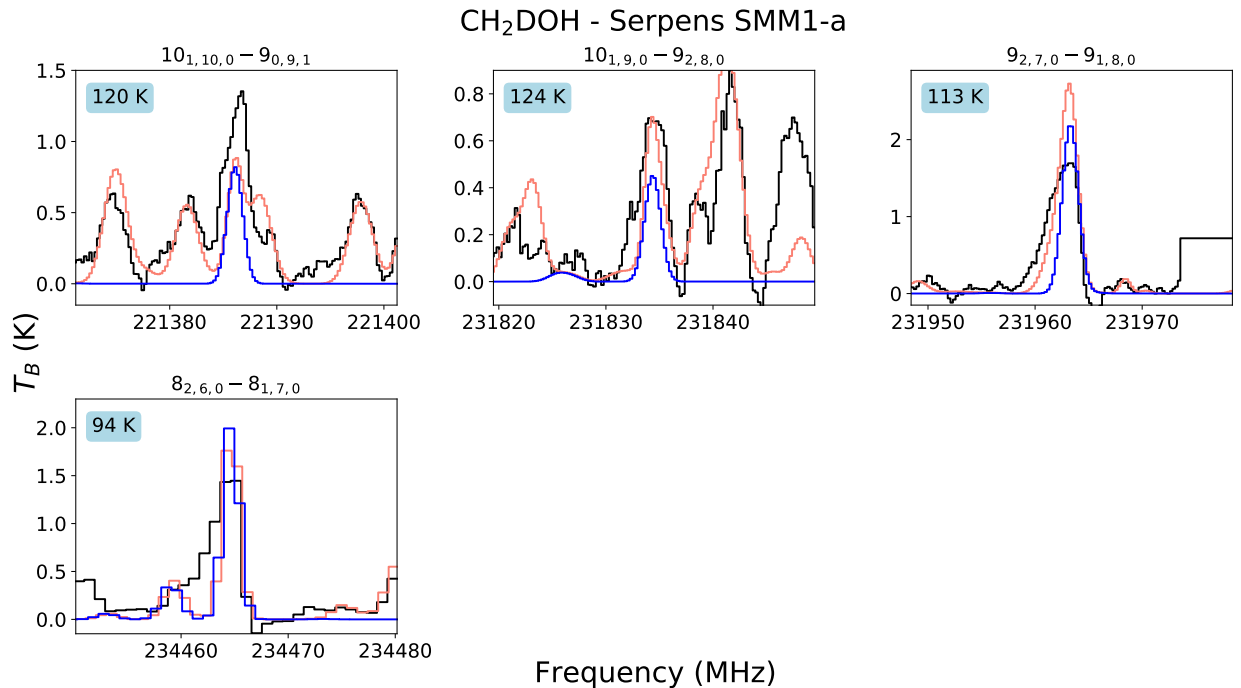


Figure 12: Identified lines of CH₂DOH toward SMM1-a. The observed spectrum is plotted in black, with the synthetic spectrum of the species overplotted in blue, and the synthetic spectrum of all fitted species combined in red. The transition is indicated at the top of each panel and the upper state energy is given in the top left of each panel.

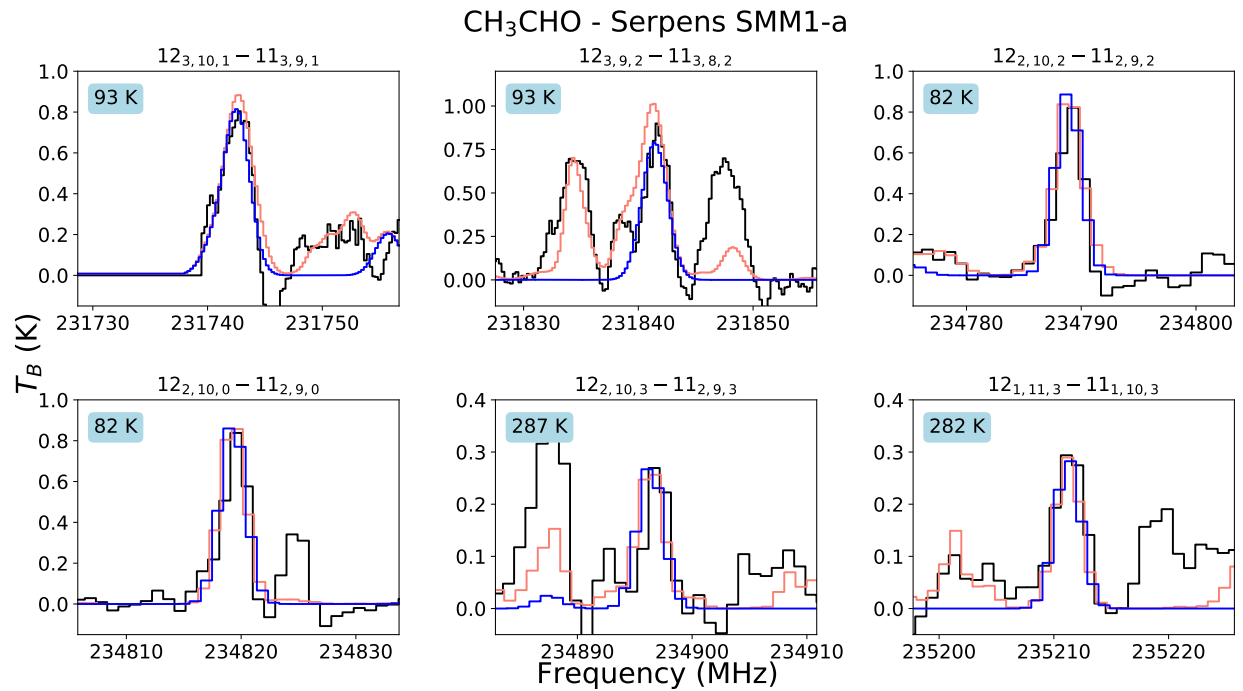


Figure 13: Identified lines of CH₃CHO toward SMM1-a. The observed spectrum is plotted in black, with the synthetic spectrum of the species overplotted in blue, and the synthetic spectrum of all fitted species combined in red. The transition is indicated at the top of each panel and the upper state energy is given in the top left of each panel.

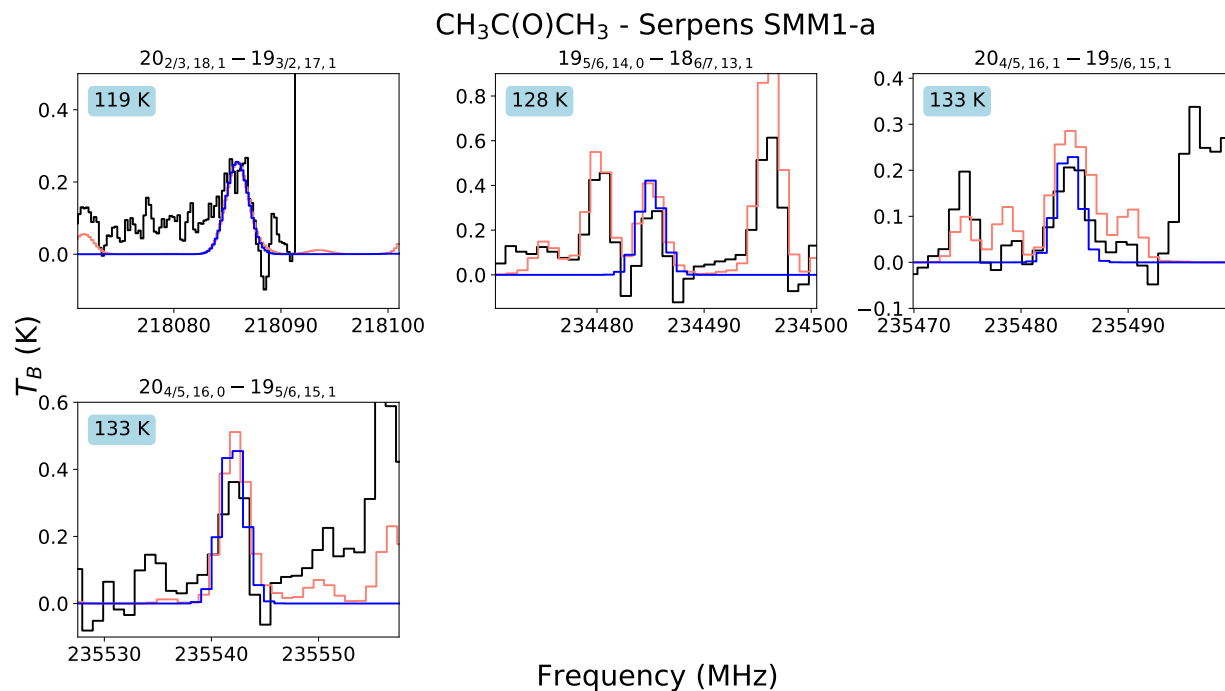


Figure 14: Identified lines of CH₃C(O)CH₃ toward SMM1-a. The observed spectrum is plotted in black, with the synthetic spectrum overlotted in blue. The transition is indicated at the top of each panel and the upper state energy is given in the top left of each panel.

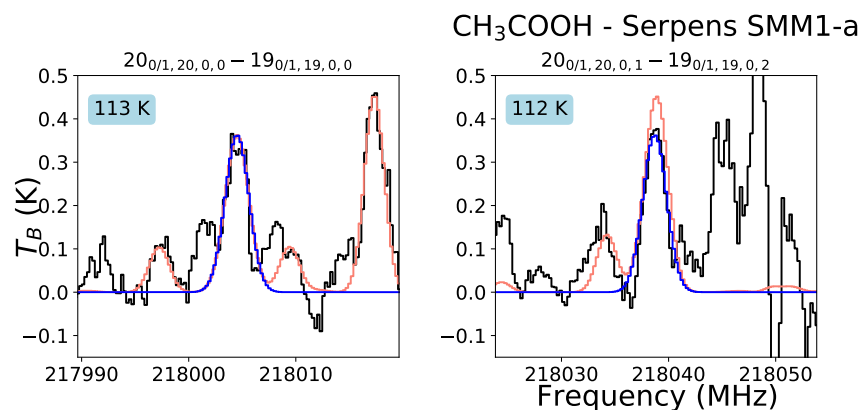


Figure 15: Identified lines of CH₃COOH toward SMM1-a. The observed spectrum is plotted in black, with the synthetic spectrum of the species overlotted in blue, and the synthetic spectrum of all fitted species combined in red. The transition is indicated at the top of each panel and the upper state energy is given in the top left of each panel.

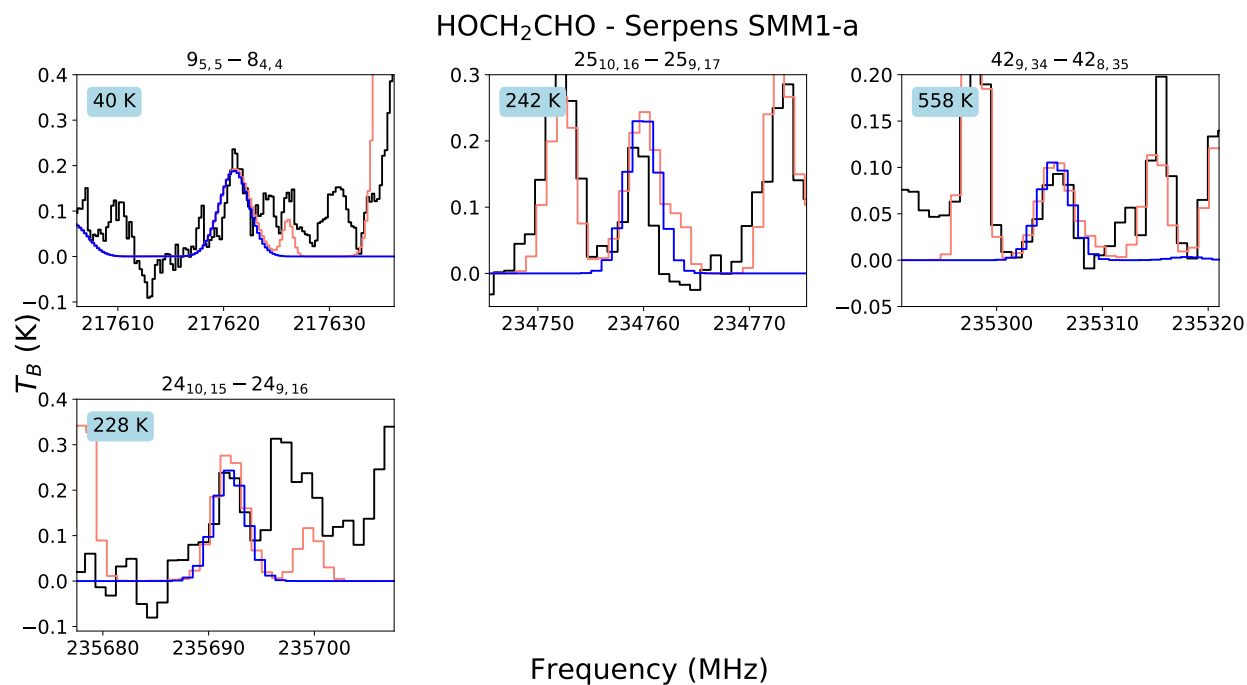


Figure 16: Identified lines of HOCH₂CHO toward SMM1-a. The observed spectrum is plotted in black, with the synthetic spectrum of the species overplotted in blue, and the synthetic spectrum of all fitted species combined in red. The transition is indicated at the top of each panel and the upper state energy is given in the top left of each panel.

Table 4: Column densities taken from studies presented in the literature.

Source	$N(\text{NH}_2\text{CHO})$	$N(\text{CH}_3\text{CHO})$	$N(\text{CH}_3\text{C}(\text{O})\text{NH}_2)$	$N(\text{CH}_3\text{NHCHO})$	$N(\text{NH}_2\text{C}(\text{O})\text{NH}_2)$
	% of H_2O	% of H_2O	% of H_2O	% of H_2O	% of H_2O
67P/C-G ^a	1	3.7	≤ 2.2	–	–
46P/Wirtanen ^b	(0.06 ± 0.01)	(0.015 ± 0.002)	–	–	–
	cm^{-2}	cm^{-2}	cm^{-2}	cm^{-2}	cm^{-2}
G+0.693 ^c	$(1.5 \pm 0.3) \times 10^{15}$	$(6.3 \pm 1.4) \times 10^{14}$	–	–	$(6.3 \pm 1.0) \times 10^{12}$
B1-c ^d	$(3.8 \pm 1.9) \times 10^{15}$	$(5.1 \pm 2.4) \times 10^{14}$	–	–	–
S68N ^d	$(9.8 \pm 4.2) \times 10^{14}$	$(2.7 \pm 0.3) \times 10^{14}$	–	–	–
Per-emb 44 ^e	$(2.5 \pm 1.7) \times 10^{16}$	$(1.9 \pm 0.7) \times 10^{15}$	–	–	–
Per-emb 12 B ^e	$(1.7 \pm 0.9) \times 10^{16}$	$(1.1 \pm 0.4) \times 10^{15}$	–	–	–
Per-emb 13 ^e	$(1.1 \pm 0.6) \times 10^{16}$	$(2.3 \pm 0.9) \times 10^{14}$	–	–	–
Per-emb 27 ^e	$(2.9 \pm 1.8) \times 10^{16}$	$(2.1 \pm 0.8) \times 10^{15}$	–	–	–
Per-emb 29 ^e	$(2.1 \pm 1.3) \times 10^{15}$	$(3.5 \pm 1.3) \times 10^{14}$	–	–	–
IRAS 16293B ^f	$(1.2 \pm 0.2) \times 10^{17}$	$(1.0 \pm 0.2) \times 10^{16}$	$\leq 2.5 \times 10^{15}$	–	–
G328 Shock-A ^g	$(3.2 \pm 0.6) \times 10^{16}$	$(9.3 \pm 1.9) \times 10^{16}$	–	–	–
G328 Shock-B ^g	$(4.0 \pm 0.8) \times 10^{16}$	$(1.6 \pm 0.3) \times 10^{17}$	–	–	–
G328 Envelope ^g	$(6.8 \pm 1.4) \times 10^{15}$	$(4.2 \pm 0.8) \times 10^{15}$	–	–	–

Continued on next page

Table 4 – Continued from previous page

Source	$N(\text{NH}_2\text{CHO})$	$N(\text{CH}_3\text{CHO})$	$N(\text{CH}_3\text{C}(\text{O})\text{NH}_2)$	$N(\text{CH}_3\text{NHCHO})$	$N(\text{NH}_2\text{C}(\text{O})\text{NH}_2)$
	cm^{-2}	cm^{-2}	cm^{-2}	cm^{-2}	cm^{-2}
W 3(H ₂ O) ^h	$(1.3 \pm 0.3) \times 10^{15}$	$(3.5 \pm 0.7) \times 10^{13}$	–	–	–
MM1-i ⁱ	–	$(5.3 \pm 0.9) \times 10^{17}$	$(4.7 \pm 0.7) \times 10^{16}$	$(7.5 \pm 2.8) \times 10^{16}$	–
MM1-ii ⁱ	–	$(1.4 \pm 0.4) \times 10^{18}$	$(7.4 \pm 1.1) \times 10^{16}$	–	–
MM1-iii ⁱ	–	$(2.0 \pm 0.3) \times 10^{18}$	$(1.7 \pm 0.4) \times 10^{17}$	–	–
MM1-iv ⁱ	–	$(8.1 \pm 1.2) \times 10^{17}$	$(4.0 \pm 1.2) \times 10^{17}$	$(1.0 \pm 0.4) \times 10^{17}$	–
MM1-v ⁱ	–	$(1.7 \pm 0.2) \times 10^{18}$	$(2.3 \pm 0.4) \times 10^{17}$	$(3.6 \pm 0.7) \times 10^{17}$	$(5.0 \pm 2.0) \times 10^{16}$
MM1-vi ⁱ	–	$(1.7 \pm 0.2) \times 10^{18}$	$(1.6 \pm 0.2) \times 10^{17}$	$(2.0 \pm 0.6) \times 10^{17}$	–
MM1-vii ⁱ	–	$(2.4 \pm 0.3) \times 10^{18}$	$(1.6 \pm 0.2) \times 10^{17}$	$(2.0 \pm 0.6) \times 10^{17}$	–
MM1-viii ⁱ	–	$(9.9 \pm 1.9) \times 10^{17}$	$(7.1 \pm 1.1) \times 10^{16}$	$(1.4 \pm 0.5) \times 10^{17}$	–
MM1-ix ⁱ	–	$(3.0 \pm 0.3) \times 10^{17}$	$(1.6 \pm 0.3) \times 10^{16}$	$(4.8 \pm 1.4) \times 10^{16}$	–
MM1-nmf ⁱ	–	$(9.9 \pm 1.9) \times 10^{17}$	$(6.8 \pm 1.3) \times 10^{16}$	$(1.0 \pm 0.5) \times 10^{17}$	–
MM2-i ⁱ	–	$(2.1 \pm 0.6) \times 10^{17}$	$(5.9 \pm 1.6) \times 10^{16}$	–	–
MM2-ii ⁱ	–	$(2.4 \pm 0.7) \times 10^{17}$	$(8.8 \pm 1.6) \times 10^{16}$	–	–
G31.41+0.31 ^j	$(1.7 \pm 0.6) \times 10^{17}$	–	$(8.0 \pm 4.0) \times 10^{16}$	$(3.7 \pm 1.6) \times 10^{16}$	–
GAL 034.3+00.2 ^k	$(5.3 \pm 0.7) \times 10^{13}$	$(1.7 \pm 0.3) \times 10^{13}$	–	–	–
Orion KL A ^l	$(1.6 \pm 0.5) \times 10^{15}$	$(4.0 \pm 1.0) \times 10^{15}$	$(1.2 \pm 0.4) \times 10^{15}$	–	–

Continued on next page

Table 4 – Continued from previous page

Source	$N(\text{NH}_2\text{CHO})$	$N(\text{CH}_3\text{CHO})$	$N(\text{CH}_3\text{C}(\text{O})\text{NH}_2)$	$N(\text{CH}_3\text{NHCHO})$	$N(\text{NH}_2\text{C}(\text{O})\text{NH}_2)$
	cm^{-2}	cm^{-2}	cm^{-2}	cm^{-2}	cm^{-2}
Orion KL B ^l	$(1.4 \pm 0.3) \times 10^{15}$	$(7.0 \pm 3.0) \times 10^{14}$	$\leq 4 \times 10^{15}$	–	–
NGC 7538 IRS1 ^h	$(5.7 \pm 1.1) \times 10^{14}$	$(2.8 \pm 0.6) \times 10^{13}$	–	–	–
NGC6334-29 ^k	$(7.6 \pm 1.1) \times 10^{13}$	$(1.3 \pm 0.3) \times 10^{13}$	–	–	–
AFGL 4176 ^m	$(1.5 \pm 0.8) \times 10^{16}$	$(1.0 \pm 0.1) \times 10^{16}$	–	–	–
GAL 31.41+0.31 ^k	$(6.4 \pm 0.6) \times 10^{13}$	$(7.1 \pm 1.0) \times 10^{12}$	–	–	–
GAL 10.47+00.03 ^k	$(6.7 \pm 0.5) \times 10^{14}$	$(1.1 \pm 0.1) \times 10^{14}$	–	–	–
G10.6-0.4 hc1 ⁿ	$(4.0 \pm 2.6) \times 10^{15}$	$(4.2 \pm 0.4) \times 10^{16}$	–	–	–
G10.6-0.4 hc2 ⁿ	$(6.3 \pm 0.4) \times 10^{15}$	$(1.3 \pm 0.2) \times 10^{16}$	–	–	–
Sgr B2(M) ^o	$(5.8 \pm 1.2) \times 10^{14}$	$(1.4 \pm 0.3) \times 10^{16}$	–	–	–
Sgr B2(N1S) ^p	$(2.9 \pm 0.9) \times 10^{18}$	–	$(4.1 \pm 1.2) \times 10^{17}$	$(2.6 \pm 0.8) \times 10^{17}$	$(2.7 \pm 0.8) \times 10^{16}$
Sgr B2(N2) ^q	$(3.5 \pm 1.1) \times 10^{18}$	$(5.3 \pm 1.1) \times 10^{17}$	$(1.4 \pm 0.7) \times 10^{17}$	$(1.0 \pm 0.2) \times 10^{17}$	–
Sgr B2(N) (1) ^o	$(1.4 \pm 0.3) \times 10^{17}$	$(1.4 \pm 0.3) \times 10^{18}$	–	–	–
Sgr B2(N) (2) ^o	$(8.0 \pm 1.6) \times 10^{16}$	$(9.0 \pm 1.8) \times 10^{17}$	–	–	–
Sgr B2(N) cold ^r	$(1.6 \pm 0.7) \times 10^{14}$	–	$(5.2 \pm 3.5) \times 10^{13}$	–	–
Sgr B2(N) warm ^r	$(4.0 \pm 1.2) \times 10^{14}$	–	$(6.4 \pm 4.7) \times 10^{14}$	–	–

Data are taken from: a^{40,41}; b¹⁰; c^{16,42,43}; d^{44,45}; e⁴⁶; f^{9,20,47}; g⁴⁸; h⁴⁹; i¹⁹; j¹⁵; k⁵⁰; l⁵¹; m⁵²; n⁵³; o⁵⁴; p¹³; q^{12,17}; r⁵⁵

References

- (1) Lucas-Lenard, J.; Lipmann, F. Protein biosynthesis. *Annual review of biochemistry* **1971**, *40*, 409–448.
- (2) McKee, A. D.; Solano, M.; Saydjari, A.; Bennett, C. J.; Hud, N. V.; Orlando, T. M. A Possible Path to Prebiotic Peptides Involving Silica and Hydroxy Acid-Mediated Amide Bond Formation. *ChemBioChem* **2018**, *19*, 1913–1917.
- (3) Imai, E.-i.; Honda, H.; Hatori, K.; Brack, A.; Matsuno, K. Elongation of oligopeptides in a simulated submarine hydrothermal system. *Science* **1999**, *283*, 831–833.
- (4) Lemke, K. H.; Rosenbauer, R. J.; Bird, D. K. Peptide synthesis in early Earth hydrothermal systems. *Astrobiology* **2009**, *9*, 141–146.
- (5) Simakov, M.; Kuzicheva, E.; Mal’Ko, I.; Dodonova, N. Y. Abiogenic synthesis of oligopeptides in solid state under action of vacuum ultraviolet light (100–200 nm). *Advances in Space Research* **1996**, *18*, 61–64.
- (6) Sugahara, H.; Mimura, K. Glycine oligomerization up to triglycine by shock experiments simulating comet impacts. *Geochemical Journal* **2014**, *48*, 51–62.
- (7) Kaiser, R.; Stockton, A.; Kim, Y.; Jensen, E.; Mathies, R. On the formation of dipeptides in interstellar model ices. *The Astrophysical Journal* **2013**, *765*, 111.
- (8) Rubin, R. H.; Swenson, J., G. W.; Benson, R. C.; Tigelaar, H. L.; Flygare, W. H. Microwave Detection of Interstellar Formamide. *The Astrophysical Journal Letters* **1971**, *169*, L39.
- (9) Coutens, A.; Jørgensen, J. K.; Van der Wiel, M. H. D.; Müller, H.; Lykke, J. M.; Bjerke, P.; Bourke, T.; Calcutt, H.; Drozdovskaya, M.; Favre, C., et al. The ALMA-PILS survey: First detections of deuterated formamide and deuterated isocyanic acid in the interstellar medium. *Astronomy & Astrophysics* **2016**, *590*, L6.

- (10) Biver, N.; Bockelée-Morvan, D.; Boissier, J.; Moreno, R.; Crovisier, J.; Lis, D.; Colom, P.; Cordiner, M.; Milam, S.; Roth, N., et al. Molecular composition of comet 46P/Wirtanen from millimetre-wave spectroscopy. *Astronomy & Astrophysics* **2021**, *648*, A49.
- (11) Hollis, J. M.; Lovas, F. J.; Remijan, A. J.; Jewell, P. R.; Ilyushin, V. V.; Kleiner, I. Detection of Acetamide (CH_3CONH_2): The Largest Interstellar Molecule with a Peptide Bond. *The Astrophysical Journal Letters* **2006**, *643*, L25–L28.
- (12) Belloche, A.; Meshcheryakov, A. A.; Garrod, R. T.; Ilyushin, V. V.; Alekseev, E. A.; Motiyenko, R. A.; Margulès, L.; Müller, H. S. P.; Menten, K. M. Rotational spectroscopy, tentative interstellar detection, and chemical modeling of N-methylformamide. *Astronomy & Astrophysics* **2017**, *601*, A49.
- (13) Belloche, A.; Garrod, R. T.; Müller, H. S. P.; Menten, K. M.; Medvedev, I.; Thomas, J.; Kisiel, Z. Re-exploring Molecular Complexity with ALMA (ReMoCA): interstellar detection of urea. *Astronomy & Astrophysics* **2019**, *628*, A10.
- (14) Ligterink, N. F.; Grimaudo, V.; Moreno-García, P.; Lukmanov, R.; Tulej, M.; Leya, I.; Lindner, R.; Wurz, P.; Cockell, C. S.; Ehrenfreund, P., et al. ORIGIN: a novel and compact Laser Desorption–Mass Spectrometry system for sensitive in situ detection of amino acids on extraterrestrial surfaces. *Scientific reports* **2020**, *10*, 1–10.
- (15) Colzi, L.; Rivilla, V.; Beltrán, M.; Jiménez-Serra, I.; Mininni, C.; Melosso, M.; Cesaroni, R.; Fontani, F.; Lorenzani, A.; Sánchez-Monge, A., et al. The GUAPOS project II. A comprehensive study of peptide-like bond molecules. *arXiv preprint arXiv:2107.11258* **2021**,
- (16) Jiménez-Serra, I.; Martín-Pintado, J.; Rivilla, V. M.; Rodríguez-Almeida, L.; Alonso Alonso, E. R.; Zeng, S.; Cocinero, E. J.; Martín, S.; Requena-Torres, M.; Martín-Domenech, R., et al. Toward the RNA-world in the interstellar

- medium—Detection of urea and search of 2-amino-oxazole and simple sugars. *Astrobiology* **2020**, *20*, 1048–1066.
- (17) Sanz-Novo, M.; Belloche, A.; Alonso, J.; Kolesníková, L.; Garrod, R.; Mata, S.; Müller, H.; Menten, K.; Gong, Y. Interstellar glycolamide: A comprehensive rotational study and an astronomical search in Sgr B2 (N). *Astronomy & Astrophysics* **2020**, *639*, A135.
- (18) Li, J.; Wang, J.; Lu, X.; Ilyushin, V.; Motiyenko, R. A.; Gou, Q.; Alekseev, E. A.; Quan, D.; Margules, L.; Gao, F., et al. Propionamide (C₂H₅CONH₂): The largest peptide-like molecule in space. *arXiv preprint arXiv:2108.05001* **2021**,
- (19) Ligterink, N. F.; El-Abd, S. J.; Brogan, C. L.; Hunter, T. R.; Remijan, A. J.; Garrod, R. T.; McGuire, B. M. The family of amide molecules toward NGC 6334I. *The Astrophysical Journal* **2020**, *901*, 37.
- (20) Ligterink, N.; Terwisscha van Scheltinga, J.; Taquet, V.; Jørgensen, J.; Cazaux, S.; van Dishoeck, E.; Linnartz, H. The formation of peptide-like molecules on interstellar dust grains. *Monthly Notices of the Royal Astronomical Society* **2018**, *480*, 3628–3643.
- (21) Ortiz-León, G. N.; Dzib, S. A.; Kounkel, M. A.; Loinard, L.; Mioduszewski, A. J.; Rodríguez, L. F.; Torres, R. M.; Pech, G.; Rivera, J. L.; Hartmann, L., et al. The Gould’s Belt Distances Survey (GOBELINS). III. The Distance to the Serpens/Aquila Molecular Complex. *The Astrophysical Journal* **2017**, *834*, 143.
- (22) Dionatos, O.; Jørgensen, J. K.; Green, J. D.; Herczeg, G.; Evans, N. J.; Kristensen, L.; Lindberg, J.; Van Dishoeck, E. Dust, ice and gas in time (DIGIT): Herschel and Spitzer spectro-imaging of SMM3 and SMM4 in Serpens. *Astronomy & Astrophysics* **2013**, *558*, A88.
- (23) Hull, C. L.; Girart, J. M.; Kristensen, L. E.; Dunham, M. M.; Rodríguez-Kamenetzky, A.; Carrasco-González, C.; Cortés, P. C.; Li, Z.-Y.; Plambeck, R. L.

- An Extremely High Velocity Molecular Jet Surrounded by an Ionized Cavity in the Protostellar Source Serpens SMM1. *The Astrophysical Journal Letters* **2016**, *823*, L27.
- (24) Öberg, K. I.; Van der Marel, N.; Kristensen, L. E.; Van Dishoeck, E. F. Complex molecules toward low-mass protostars: the Serpens core. *The Astrophysical Journal* **2011**, *740*, 14.
- (25) Goicoechea, J. R.; Cernicharo, J.; Karska, A.; Herczeg, G.; Polehampton, E.; Wampfler, S. F.; Kristensen, L.; Van Dishoeck, E.; Etxaluze, M.; Berné, O., et al. The complete far-infrared and submillimeter spectrum of the Class 0 protostar Serpens SMM1 obtained with Herschel-Characterizing UV-irradiated shocks heating and chemistry. *Astronomy & Astrophysics* **2012**, *548*, A77.
- (26) Ligterink, N.; Ahmadi, A.; Coutens, A.; Calcutt, H.; van Dishoeck, E.; Linnartz, H.; Jørgensen, J.; Garrod, R.; Bouwman, J., et al. The prebiotic molecular inventory of Serpens SMM1-I. An investigation of the isomers CH₃NCO and HOCH₂CN. *Astronomy & Astrophysics* **2021**, *647*, A87.
- (27) Tychoniec, Ł.; van Dishoeck, E. F.; van't Hoff, M. L.; van Gelder, M. L.; Tabone, B.; Chen, Y.; Harsono, D.; Hull, C. L.; Hogerheijde, M. R.; Murillo, N. M., et al. Which molecule traces what: chemical diagnostics of protostellar sources. *arXiv preprint arXiv:2107.03696* **2021**,
- (28) Vastel, C.; Bottinelli, S.; Caux, E.; Glorian, J.; Boiziot, M. CASSIS: A tool to visualize and analyse instrumental and synthetic spectra. SF2A-2015: Proceedings of the Annual meeting of the French Society of Astronomy and Astrophysics. 2015; pp 313–316.
- (29) Müller, H. S.; Thorwirth, S.; Roth, D.; Winnewisser, G. The Cologne database for molecular spectroscopy, CDMS. *Astronomy & Astrophysics* **2001**, *370*, L49–L52.

- (30) Müller, H. S.; Schlöder, F.; Stutzki, J.; Winnewisser, G. The Cologne Database for Molecular Spectroscopy, CDMS: a useful tool for astronomers and spectroscopists. *Journal of Molecular Structure* **2005**, *742*, 215–227.
- (31) Endres, C. P.; Schlemmer, S.; Schilke, P.; Stutzki, J.; Müller, H. S. The cologne database for molecular spectroscopy, CDMS, in the virtual atomic and molecular data centre, VAMDC. *Journal of Molecular Spectroscopy* **2016**, *327*, 95–104.
- (32) Pickett, H.; Poynter, R.; Cohen, E.; Delitsky, M.; Pearson, J.; Müller, H. Submillimeter, millimeter, and microwave spectral line catalog. *Journal of Quantitative Spectroscopy and Radiative Transfer* **1998**, *60*, 883–890.
- (33) Schuller, F.; Menten, K.; Contreras, Y.; Wyrowski, F.; Schilke, P.; Bronfman, L.; Henning, T.; Walmsley, C.; Beuther, H.; Bontemps, S., et al. ATLASGAL—The APEX telescope large area survey of the galaxy at 870 μ m. *Astronomy & Astrophysics* **2009**, *504*, 415–427.
- (34) Ahmadi, A.; Beuther, H.; Mottram, J.; Bosco, F.; Linz, H.; Henning, T.; Winters, J.; Kuiper, R.; Pudritz, R.; Sánchez-Monge, Á., et al. Core fragmentation and Toomre stability analysis of W3 (H₂O)-A case study of the IRAM NOEMA large program CORE. *Astronomy & Astrophysics* **2018**, *618*, A46.
- (35) Ossenkopf, V.; Henning, T. Dust opacities for protostellar cores. *Astronomy and Astrophysics* **1994**, *291*, 943–959.
- (36) Calcutt, H.; Viti, S.; Codella, C.; Beltrán, M. T.; Fontani, F.; Woods, P. M. A high-resolution study of complex organic molecules in hot cores. *Monthly Notices of the Royal Astronomical Society* **2014**, *443*, 3157–3173.
- (37) Wilson, T. Isotopes in the interstellar medium and circumstellar envelopes. *Reports on Progress in Physics* **1999**, *62*, 143.

- (38) Yan, Y.; Zhang, J.; Henkel, C.; Mufakharov, T.; Jia, L.; Tang, X.; Wu, Y.; Li, J.; Zeng, Z.; Wang, Y., et al. A Systematic TMRT Observational Study of Galactic $^{12}\text{C}/^{13}\text{C}$ Ratios from Formaldehyde. *The Astrophysical Journal* **2019**, *877*, 154.
- (39) Zeng, S.; Zhang, Q.; Jiménez-Serra, I.; Tercero, B.; Lu, X.; Martín-Pintado, J.; De Vicente, P.; Rivilla, V.; Li, S. Cloud–cloud collision as drivers of the chemical complexity in Galactic Centre molecular clouds. *Monthly Notices of the Royal Astronomical Society* **2020**, *497*, 4896–4909.
- (40) Goesmann, F.; Rosenbauer, H.; Bredehöft, J. H.; Cabane, M.; Ehrenfreund, P.; Gautier, T.; Giri, C.; Krüger, H.; Le Roy, L.; MacDermott, A. J., et al. Organic compounds on comet 67P/Churyumov-Gerasimenko revealed by COSAC mass spectrometry. *Science* **2015**, *349*, aab0689.
- (41) Altwegg, K.; Balsiger, H.; Berthelier, J.-J.; Bieler, A.; Calmonte, U.; Fuselier, S. A.; Goesmann, F.; Gasc, S.; Gombosi, T. I.; Le Roy, L., et al. Organics in comet 67P—a first comparative analysis of mass spectra from ROSINA–DFMS, COSAC and Ptolemy. *Monthly Notices of the Royal Astronomical Society* **2017**, *469*, S130–S141.
- (42) Requena-Torres, M.; Martín-Pintado, J.; Martín, S.; Morris, M. The galactic center: The largest oxygen-bearing organic molecule repository. *The Astrophysical Journal* **2008**, *672*, 352.
- (43) Zeng, S.; Jiménez-Serra, I.; Rivilla, V.; Martín, S.; Martín-Pintado, J.; Requena-Torres, M.; Armijos-Abendaño, J.; Riquelme, D.; Aladro, R. Complex organic molecules in the Galactic Centre: the N-bearing family. *Monthly Notices of the Royal Astronomical Society* **2018**, *478*, 2962–2975.
- (44) van Gelder, M.; Tabone, B.; van Dishoeck, E.; Beuther, H.; Boogert, A.; Garatti, A. C.; Klaassen, P.; Linnartz, H.; Müller, H.; Taquet, V., et al. Complex

- organic molecules in low-mass protostars on Solar System scales-I. Oxygen-bearing species. *Astronomy & Astrophysics* **2020**, *639*, A87.
- (45) Nazari, P.; van Gelder, M.; van Dishoeck, E.; Tabone, B.; van't Hoff, M.; Ligterink, N.; Beuther, H.; Boogert, A.; Caratti o Garatti, A.; Klaassen, P., et al. Complex organic molecules in low-mass protostars on Solar System scales: II. Nitrogen-bearing species. *Astronomy & Astrophysics* **2021**, *650*, A150.
- (46) Yang, Y.-L.; Sakai, N.; Zhang, Y.; Murillo, N. M.; Zhang, Z. E.; Higuchi, A. E.; Zeng, S.; López-Sepulcre, A.; Yamamoto, S.; Lefloch, B., et al. The Perseus ALMA Chemistry Survey (PEACHES). I. The Complex Organic Molecules in Perseus Embedded Protostars. *The Astrophysical Journal* **2021**, *910*, 20.
- (47) Lykke, J.; Coutens, A.; Jørgensen, J.; Van der Wiel, M.; Garrod, R.; Müller, H.; Bjerkeli, P.; Bourke, T.; Calcutt, H.; Drozdovskaya, M., et al. The ALMA-PILS survey: First detections of ethylene oxide, acetone and propanal toward the low-mass protostar IRAS 16293-2422. *Astronomy & Astrophysics* **2017**, *597*, A53.
- (48) Csengeri, T.; Belloche, A.; Bontemps, S.; Wyrowski, F.; Menten, K.; Bouscasse, L. Search for high-mass protostars with ALMA revealed up to kilo-parsec scales (SPARKS)-II. Complex organic molecules and heavy water in shocks around a young high-mass protostar. *Astronomy & Astrophysics* **2019**, *632*, A57.
- (49) Bisschop, S.; Jørgensen, J.; Van Dishoeck, E.; De Wachter, E. Testing grain-surface chemistry in massive hot-core regions. *Astronomy & Astrophysics* **2007**, *465*, 913–929.
- (50) Weaver, S. L. W.; Laas, J. C.; Zou, L.; Kroll, J. A.; Rad, M. L.; Hays, B. M.; Sanders, J. L.; Lis, D. C.; Cross, T. N.; Wehres, N., et al. Deep, broadband spectral line surveys of molecule-rich interstellar clouds. *The Astrophysical Journal Supplement Series* **2017**, *232*, 3.

- (51) Cernicharo, J.; Kisiel, Z.; Tercero, B.; Kolesniková, L.; Medvedev, I.; López, A.; Fortman, S.; Winnewisser, M.; De Lucia, F.; Alonso, J., et al. A rigorous detection of interstellar CH₃NCO: an important missing species in astrochemical networks. *Astronomy & Astrophysics* **2016**, *587*, L4.
- (52) Bøgelund, E. G.; Barr, A. G.; Taquet, V.; Ligterink, N. F. W.; Persson, M. V.; Hogerheijde, M. R.; van Dishoeck, E. F. Molecular complexity on disc scales uncovered by ALMA. Chemical composition of the high-mass protostar AFGL 4176. *Astronomy & Astrophysics* **2019**, *628*, A2.
- (53) Law, C. J.; Zhang, Q.; Öberg, K. I.; Galván-Madrid, R.; Keto, E.; Liu, H. B.; Ho, P. T. Subarcsecond Imaging of the Complex Organic Chemistry in Massive Star-forming Region G10. 6-0.4. *The Astrophysical Journal* **2021**, *909*, 214.
- (54) Belloche, A.; Müller, H. S.; Menten, K. M.; Schilke, P.; Comito, C. Complex organic molecules in the interstellar medium: IRAM 30 m line survey of Sagittarius B2 (N) and (M). *Astronomy & Astrophysics* **2013**, *559*, A47.
- (55) Halfen, D. T.; Ilyushin, V.; Ziurys, L. M. Formation of Peptide Bonds in Space: A Comprehensive Study of Formamide and Acetamide in Sgr B2(N). *The Astrophysical Journal* **2011**, *743*, 60.
- (56) Jacobsen, S.; Jørgensen, J.; Van der Wiel, M.; Calcutt, H.; Bourke, T.; Brinch, C.; Coutens, A.; Drozdovskaya, M. N.; Kristensen, L.; Müller, H., et al. The ALMA-PILS survey: 3D modeling of the envelope, disks and dust filament of IRAS 16293–2422. *Astronomy & Astrophysics* **2018**, *612*, A72.
- (57) Quénard, D.; Jiménez-Serra, I.; Viti, S.; Holdship, J.; Coutens, A. Chemical modelling of complex organic molecules with peptide-like bonds in star-forming regions. *Monthly Notices of the Royal Astronomical Society* **2018**, *474*, 2796–2812.

- (58) Charnley, S. Acetaldehyde in star-forming regions. *Advances in Space Research* **2004**, *33*, 23–30.
- (59) Garrod, R. T.; Jin, M.; Matis, K. A.; Jones, D.; Willis, E. R.; Herbst, E. Formation of complex organic molecules in hot molecular cores through nondiffusive grain-surface and ice-mantle chemistry. *arXiv preprint arXiv:2110.09743* **2021**,
- (60) Codella, C.; Ceccarelli, C.; Caselli, P.; Balucani, N.; Barone, V.; Fontani, F.; Lefloch, B.; Podio, L.; Viti, S.; Feng, S., et al. Seeds of Life in Space (SOLIS)-II. Formamide in protostellar shocks: Evidence for gas-phase formation. *Astronomy & Astrophysics* **2017**, *605*, L3.
- (61) Quan, D.; Herbst, E. Possible gas-phase syntheses for seven neutral molecules studied recently with the Green Bank Telescope. *Astronomy & Astrophysics* **2007**, *474*, 521–527.
- (62) Redondo, P.; Barrientos, C.; Largo, A. Peptide bond formation through gas-phase reactions in the interstellar medium: formamide and acetamide as prototypes. *The Astrophysical Journal* **2014**, *793*, 32.
- (63) Yang, Z.; Pan, N. Computational studies of ion–neutral reactions of astrochemical relevance: Formation of hydrogen peroxide, acetamide, and amino acetonitrile. *International Journal of Mass Spectrometry* **2015**, *378*, 364–368.
- (64) Foo, L.; Surányi, A.; Guljas, A.; Szőri, M.; Villar, J. J.; Viskolcz, B.; Csizmadia, I. G.; Rágyanszki, A.; Fiser, B. Formation of acetamide in interstellar medium. *Molecular Astrophysics* **2018**, *13*, 1–5.
- (65) Kothari, A.; Zhu, L.; Babi, J.; Galant, N.; Rágyanszki, A.; Csizmadia, I. Ketene and Ammonia Forming Acetamide in the Interstellar Medium. *Journal of Undergraduate Life Sciences* **2020**, *14*.

- (66) Berger, R. The proton irradiation of methane, ammonia, and water at 77 K. *Proceedings of the National Academy of Sciences of the United States of America* **1961**, *47*, 1434.
- (67) Bernstein, M. P.; Sandford, S. A.; Allamandola, L. J.; Chang, S.; Scharberg, M. A. Organic compounds produced by photolysis of realistic interstellar and cometary ice analogs containing methanol. *The Astrophysical Journal* **1995**, *454*, 327.
- (68) Henderson, B. L.; Gudipati, M. S. Direct detection of complex organic products in ultraviolet ($\text{Ly}\alpha$) and electron-irradiated astrophysical and cometary ice analogs using two-step laser ablation and ionization mass spectrometry. *The Astrophysical Journal* **2015**, *800*, 66.
- (69) Agarwal, V.; Schutte, W.; Greenberg, J.; Ferris, J.; Briggs, R.; Connor, S.; Van de Bult, C.; Baas, F. Photochemical reactions in interstellar grains photolysis of CO, NH_3 , and H_2O . *Origins of Life and Evolution of the Biosphere* **1985**, *16*, 21–40.
- (70) Rimola, A.; Skouteris, D.; Balucani, N.; Ceccarelli, C.; Enrique-Romero, J.; Taquet, V.; Ugliengo, P. Can formamide be formed on interstellar ice? An atomistic perspective. *ACS Earth and Space Chemistry* **2018**, *2*, 720–734.
- (71) Haupa, K. A.; Tarczay, G.; Lee, Y.-P. Hydrogen abstraction/addition tunneling reactions elucidate the interstellar $\text{H}_2\text{NCHO}/\text{HNCO}$ ratio and H_2 formation. *Journal of the American Chemical Society* **2019**, *141*, 11614–11620.
- (72) Bulak, M.; Paardekooper, D.; Fedoseev, G.; Linnartz, H. Photolysis of acetonitrile in a water-rich ice as a source of complex organic molecules: CH_3CN and H_2O : CH_3CN ices. *Astronomy & Astrophysics* **2021**, *647*, A82.
- (73) Duvernay, F.; Dufaure, V.; Danger, G.; Theulé, P.; Borget, F.; Chiavassa, T. Chiral molecule formation in interstellar ice analogs: α -aminoethanol $\text{NH}_2\text{CH}(\text{CH}_3)\text{OH}$. *Astronomy & Astrophysics* **2010**, *523*, A79.

- (74) Haupa, K. A.; Ong, W.-S.; Lee, Y.-P. Hydrogen abstraction in astrochemistry: formation of CH_2CONH_2 in the reaction of H atom with acetamide (CH_3CONH_2) and photolysis of CH_2CONH_2 to form ketene (CH_2CO) in solid para-hydrogen. *Physical Chemistry Chemical Physics* **2020**, *22*, 6192–6201.
- (75) Lopez-Sepulcre, A.; Balucani, N.; Ceccarelli, C.; Codella, C.; Dulieu, F.; Theule, P. Interstellar formamide (NH_2CHO), a key prebiotic precursor. *ACS Earth and Space Chemistry* **2019**, *3*, 2122–2137.
- (76) Tielens, A. Surface chemistry of deuterated molecules. *Astronomy and Astrophysics* **1983**, *119*, 177–184.
- (77) Skouteris, D.; Vazart, F.; Ceccarelli, C.; Balucani, N.; Puzzarini, C.; Barone, V. New quantum chemical computations of formamide deuteration support gas-phase formation of this prebiotic molecule. *Monthly Notices of the Royal Astronomical Society: Letters* **2017**, *468*, L1–L5.
- (78) Fedoseev, G.; Chuang, K.-J.; van Dishoeck, E. F.; Ioppolo, S.; Linnartz, H. Simultaneous hydrogenation and UV-photolysis experiments of NO in CO-rich interstellar ice analogues; linking HNC, OCN-, NH_2CHO , and NH_2OH . *Monthly Notices of the Royal Astronomical Society* **2016**, *460*, 4297–4309.
- (79) Milam, S. N.; Savage, C.; Brewster, M. A.; Ziurys, L. M.; Wyckoff, S. The $^{12}\text{C}/^{13}\text{C}$ Isotope Gradient Derived from Millimeter Transitions of CN: The Case for Galactic Chemical Evolution. *The Astrophysical Journal* **2005**, *634*, 1126–1132.
- (80) Frigge, R.; Zhu, C.; Turner, A. M.; Abplanalp, M. J.; Bergantini, A.; Sun, B.-J.; Chen, Y.-L.; Chang, A. H.; Kaiser, R. I. A Vacuum Ultraviolet Photoionization Study on the Formation of N-methyl Formamide (HCONHCH_3) in Deep Space: A Potential Interstellar Molecule with a Peptide Bond. *The Astrophysical Journal* **2018**, *862*, 84.

- (81) Booth, A. S.; Walsh, C.; van Scheltinga, J. T.; van Dishoeck, E. F.; Ilee, J. D.; Hogerheijde, M. R.; Kama, M.; Nomura, H. An inherited complex organic molecule reservoir in a warm planet-hosting disk. *Nature Astronomy* **2021**, 1–7.
- (82) Drozdovskaya, M. N.; van Dishoeck, E. F.; Rubin, M.; Jørgensen, J. K.; Altwegg, K. Ingredients for solar-like systems: protostar IRAS 16293-2422 B versus comet 67P/Churyumov–Gerasimenko. *Monthly Notices of the Royal Astronomical Society* **2019**, *490*, 50–79.
- (83) Belloche, A.; Maury, A.; Maret, S.; Anderl, S.; Bacmann, A.; André, P.; Bontemps, S.; Cabrit, S.; Codella, C.; Gaudel, M., et al. Questioning the spatial origin of complex organic molecules in young protostars with the CALYPSO survey. *Astronomy & Astrophysics* **2020**,
- (84) Chyba, C.; Sagan, C. Endogenous production, exogenous delivery and impact-shock synthesis of organic molecules: an inventory for the origins of life. *Nature* **1992**, *355*, 125–132.
- (85) Pearson, J. C.; Yu, S.; Drouin, B. J. The ground state torsion rotation spectrum of CH₂DOH. *Journal of Molecular Spectroscopy* **2012**, *280*, 119–133.
- (86) Jacq, T.; Walmsley, C.; Mauersberger, R.; Anderson, T.; Herbst, E.; De Lucia, F. Detection of interstellar CH₂DOH. *Astronomy and Astrophysics* **1993**, *271*, 276.
- (87) Quade, C. R.; Suenram, R. The microwave spectrum of CH₂DOH. *The Journal of Chemical Physics* **1980**, *73*, 1127–1131.
- (88) Mukhopadhyay, I.; Sastry, K. Q-branch microwave transitions in the torsional ground state of methanol-D1. *Spectrochimica Acta Part A: Molecular and Biomolecular Spectroscopy* **1997**, *53*, 2061–2065.

- (89) Su, C. F.; Quade, C. R. Microwave detection of direct trans to gauche transitions in CH₂DOH. *Journal of Molecular Spectroscopy* **1989**, *134*, 290–296.
- (90) El Hilali, A.; Coudert, L.; Konov, I.; Klee, S. Analysis of the torsional spectrum of monodeuterated methanol CH₂DOH. *The Journal of chemical physics* **2011**, *135*, 194309.
- (91) Johnson, H.; Strandberg, M. The Microwave Spectrum of Ketene. *The Journal of Chemical Physics* **1952**, *20*, 687–695.
- (92) Fabricant, B.; Krieger, D.; Muentner, J. Molecular beam electric resonance study of formaldehyde, thioformaldehyde, and ketene. *The Journal of Chemical Physics* **1977**, *67*, 1576–1586.
- (93) Brown, R. D.; Godfrey, P. D.; McNaughton, D.; Pierlot, A. P.; Taylor, W. H. Microwave spectrum of ketene. *Journal of Molecular Spectroscopy* **1990**, *140*, 340–352.
- (94) Kleiner, I.; Lovas, F. J.; Godefroid, M. Microwave spectra of molecules of astrophysical interest. XXIII. Acetaldehyde. *Journal of Physical and Chemical Reference Data* **1996**, *25*, 1113–1210.
- (95) Motiyenko, R.; Tercero, B.; Cernicharo, J.; Margulès, L. Rotational spectrum of formamide up to 1 THz and first ISM detection of its ν_{12} vibrational state. *Astronomy & Astrophysics* **2012**, *548*, A71.
- (96) Kryvda, A.; Gerasimov, V.; Dyubko, S.; Alekseev, E.; Motiyenko, R. New measurements of the microwave spectrum of formamide. *Journal of Molecular Spectroscopy* **2009**, *254*, 28–32.
- (97) Blanco, S.; López, J. C.; Lesarri, A.; Alonso, J. L. Microsolvation of formamide: a rotational study. *Journal of the American Chemical Society* **2006**, *128*, 12111–12121.

- (98) Vorob'eva, E.; Dyubko, S. Submillimeter rotational spectrum of the formamide molecule: Ground and first excited vibrational states. *Radiophysics and quantum electronics* **1994**, *37*, 155–158.
- (99) Moskienko, E.; Dyubko, S. Submillimeter rotational spectrum of formamide in the ground vibrational state. *Radiophysics and quantum electronics* **1991**, *34*, 181–183.
- (100) Gardner, F.; Godfrey, P.; Williams, D. Observations of the ^{12}C and ^{13}C isotopes of formamide at 19 cm. *Monthly Notices of the Royal Astronomical Society* **1980**, *193*, 713–721.
- (101) Hirota, E.; Sugisaki, R.; Nielsen, C. J.; Sørensen, G. O. Molecular structure and internal motion of formamide from microwave spectrum. *Journal of Molecular Spectroscopy* **1974**, *49*, 251–267.
- (102) Kukolich, S. G.; Nelson, A. High resolution rotational spectra of formamide. *Chemical Physics Letters* **1971**, *11*, 383–384.
- (103) Kutsenko, A.; Motiyenko, R.; Margulès, L.; Guillemin, J.-C. The extended spectroscopic database for deuterated species of formamide up to 1 THz. *Astronomy & Astrophysics* **2013**, *549*, A128.
- (104) Peter, R.; Dreizler, H. Das Mikrowellenspektrum von Aceton im Torsionsgrundzustand. *Zeitschrift für Naturforschung A* **1965**, *20*, 301–312.
- (105) Vacherand, J.; Van Eijck, B.; Burie, J.; Demaison, J. The rotational spectrum of acetone: internal rotation and centrifugal distortion analysis. *Journal of Molecular Spectroscopy* **1986**, *118*, 355–362.
- (106) Oldag, F.; Sutter, D. H. The Rotational Zeeman Effect in Acetone, its g-Tensor, its Magnetic Susceptibility Anisotropics and its Molecular Electric Quadrupole Moment

- Tensor; A High Resolution Microwave Fourier Transform Study. *Zeitschrift für Naturforschung A* **1992**, *47*, 527–532.
- (107) Groner, P.; Albert, S.; Herbst, E.; De Lucia, F. C.; Lovas, F. J.; Drouin, B. J.; Pearson, J. C. Acetone: laboratory assignments and predictions through 620 GHz for the vibrational-torsional ground state. *The Astrophysical Journal Supplement Series* **2002**, *142*, 145.
- (108) Ilyushin, V. V.; Alekseev, E. A.; Dyubko, S. F.; Kleiner, I.; Hougen, J. T. Ground and first excited torsional states of acetamide. *Journal of Molecular Spectroscopy* **2004**, *227*, 115–139.
- (109) Ilyushin, V. V.; Endres, C. P.; Lewen, F.; Schlemmer, S.; Drouin, B. J. Submillimeter wave spectrum of acetic acid. *Journal of Molecular Spectroscopy* **2013**, *290*, 31–41.
- (110) Remijan, A. J.; Snyder, L. E.; McGuire, B. A.; Kuo, H.-L.; Looney, L. W.; Friedel, D. N.; Golubiatnikov, G. Y.; Lovas, F. J.; Ilyushin, V. V.; Alekseev, E. A.; Dyubko, S. F.; McCall, B. J.; Hollis, J. M. Observational Results of a Multi-telescope Campaign in Search of Interstellar Urea [(NH₂)₂CO]. *The Astrophysical Journal* **2014**, *783*, 77.
- (111) Brown, R.; Godfrey, P.; Storey, J. The microwave spectrum of urea. *Journal of Molecular Spectroscopy* **1975**, *58*, 445–450.
- (112) Kasten, W.; Dreizler, H. A highly resolved rotational transition of urea measured for radioastronomical searches. Analysis of the nitrogen quadrupole coupling. *Zeitschrift für Naturforschung A* **1986**, *41*, 1173–1174.
- (113) Kretschmer, U.; Consalvo, D.; Knaack, A.; Schade, W.; Stahl, W.; Dreizler, H. The ¹⁴N quadrupole hyperfine structure in the rotational spectrum of laser vaporized urea observed by molecular beam Fourier transform microwave spectroscopy. *Molecular Physics* **1996**, *87*, 1159–1168.

- (114) Christiansen, J. J. The microwave spectrum of cyanofornamide. *Journal of Molecular Spectroscopy* **2005**, *231*, 131–136.
- (115) Winnewisser, M.; Medvedev, I. R.; De Lucia, F. C.; Herbst, E.; Koput, J.; Sastry, K.; Butler, R. A. The millimeter-and submillimeter-wave spectrum of cyanofornamide. *The Astrophysical Journal Supplement Series* **2005**, *159*, 189.